Building and Environment 294 (2026) 114360

Contents lists available at ScienceDirect

Building and Environment

journal homepage: www.elsevier.com/locate/buildenv

Experimental study on airflow-induced particle resuspension from carpet under floor-supply displacement ventilation

Jun Yoshihara [a,*], Toshio Yamanaka [a], Tomohiro Kobayashi [a], Haruna Yamasawa [a], Noriaki Kobayashi [a], Hisako Nagata [b], Shigeru Okamoto [b]

[a] Department of Architectural Engineering, Graduate School of Engineering, The University of Osaka, 2-1 Yamadaoka, Suita, Osaka, 565-0871, Japan
[b] TOHATA ARCHITECTS & ENGINEERS, INC., 2-6-10, Koraibashi, Chuo-ku, Osaka, 541-0043, Japan

ARTICLE INFO

Keywords:
Floor-supply displacement ventilation (FSDV),
Circular ceiling diffuser (Anemostat diffuser)
Airflow-induced particle resuspension
Air-permeable carpet
Infection control

ABSTRACT

Application of floor-supply displacement ventilation (FSDV) in medical facilities remains limited due to concerns about particle resuspension, including infectious droplets and dust from shoes. However, research data on this phenomenon under FSDV airflow are scarce. This study aimed to quantitatively evaluate particle resuspension under FSDV conditions and compare it with a circular ceiling diffuser (CCD) system. Experiments were conducted in a cleanroom chamber. For FSDV, the floor supply velocity (v_f = 0.040, 0.030, and 0.010 m/s) and relative humidity (20%, 50%, and 80%) were varied. For CCD, the airflow rate (850, 750, and 250 m^3/h) was varied at 50% relative humidity. Particle concentrations were measured using particle counters to calculate resuspension rates. Microscopic observations of carpet fibers above perforations were also performed to assess microscale resuspension behavior.

Both supply velocity and humidity significantly affected resuspension under FSDV. The resuspension rate ranged from 10^{-7}–10^{-4} h^{-1} (v_f = 0.040 m/s, 50 ACH) and 10^{-8}–10^{-5} h^{-1} (v_f = 0.010 m/s, 12 ACH), showing that higher velocity and lower humidity enhanced resuspension. The resuspension rate increased with particle size, and large agglomerates (>10 μm) observed microscopically were more likely to detach due to greater exposed surface area to upward airflow. Under CCD, rates ranged from 10^{-5}–10^{-3} h^{-1} for 0.3–3 μm particles but were near zero for ≥10 μm. Airflow-induced resuspension under FSDV was smaller than that reported for walking-induced resuspension, even under high air exchange rates. This indicates that FSDV does not inherently increase resuspension risk under the tested conditions.

Abbreviations and nomenclature

Abbreviations

FSDV	Floor-supply displacement ventilation
CCD	Circular ceiling diffuser
AIIRs	Airborne infection isolation rooms
UFAD	Underfloor air distribution system
SFD	Swirling flow-type floor diffuser
HFD	Horizontal flow-type floor diffuser
CFD	Computational fluid dynamics
HEPA	High efficiency particulate air
CAV	Constant air volume
ATD	Arizona Test Dust
RKS	Ryukakusan
RH	Relative Humidity
ACH	Air changes per hour

(*continued on next column*)

(*continued*)

Nomenclature

e_s (T)	Saturation vapor pressure	[hPa]
T	Dry-bulb temperature	[K]
A_1-A_6	Empirical constants (reported by Hyland and Wexler (1983) [1])	[-]
e	Water vapor pressure	[hPa]
RH	Relative humidity	[%]
AH	Absolute humidity	[g/m^3]
v_f	Area-averaged supply air velocity over flow-through panels	[m/s]
r_d	Dynamic pressure ratio relative to v_f =0.010 m/s	[-]
Q_e	Exhaust airflow rate	[m^3/h]
A	Air change rate	[h^{-1}]
τ_n	Nominal time constant	[min]

(*continued on next page*)

* Corresponding author.
E-mail address: yoshihara_jun@arch.eng.osaka-u.ac.jp (J. Yoshihara).

https://doi.org/10.1016/j.buildenv.2026.114360
Received 22 October 2025; Received in revised form 31 January 2026; Accepted 11 February 2026
Available online 13 February 2026

(*continued*)

t_e	Duration of carpet exposure to airflow	[min]
L_{total}	Total applied mass of particles on the carpet (1.000 ± 0.020)	[g]
r_j	Resuspension rate (coefficient) for each particle size range j	[h^{-1}]
R_j	Resuspension amount per unit time for size range j	[g/h]
L_j	Deposited particle mass on the carpet (i.e., particle loading) for size range j	[g]
α	Conversion factor accounting for the total resuspension amount (210.2, 157.7, and 52.6 for v_f = 0.040, 0.030, and 0.010 m/s)	[-]
$N'_{pc,i,j}$	Number of particles measured at time step i for size range j, with the 10-minute average value prior to operator entry subtracted	[-]
V_j	Representative particle volume for size range j	[m^3]
ρ_p	Particle density (2.83 for Ryukakusan)	[g/m^3]
Δt	Duration of each time step (constant within each test case; 6 s for flow rates of 1000, 850, and 750 m^3/h, and 12 s for 250 m^3/h)	[s]
n	Total number of time steps (total number of data points)	[-]
Q_{ca}	Airflow volume per 500×500 mm air-permeable carpet tile	[m^3/h]
q_{pc}	Suction flow rate of particle counter (0.170)	[m^3/h]
$N_{pc,i,j}$	Number of particles measured at time step i for size range j	[-]
$\overline{N_{pcb,j}}$	Average number of particles measured during the 10 min before operator entry, for size range j	[-]
V_r	Room volume (20.06)	[m^3]
f_p	Mass fraction of test particles in each particle size class	[–]
m_p	Mass of a single particle	[kg]
F_D	Aerodynamic drag force acting on a particle	[N]
F_G	Gravitational force acting on a particle	[N]
C_D	Drag coefficient	[–]
A_p	Projected cross-sectional area of a particle (= πD_p^2 / 4)	[m^2]
ρ_f	Air density	[kg/m^3]
v_r	Relative velocity between the particle and the surrounding airflow (the surrounding airflow was assumed to be zero when calculating v_g)	[m/s]
Re_p	Particle Reynolds number (= $\rho_f D_p v_r / \mu$)	[-]
D_p	Particle diameter	[m]
μ	Dynamic viscosity of air	[Pa·s]
v_g	Terminal settling velocity of a particle under gravity	[m/s]
ρ_p	Particle density	[kg/m^3]
g	Gravitational acceleration (9.81)	[m/s^2]
v_u	Area-averaged supply air velocity in FSDV	[m/s]
A_c	Floor area of the test chamber, including non–flow-through panels	[m^2]
t_c	Estimated time required for a particle to reach the ceiling (outlet)	[s]
H_c	Ceiling height of the chamber	[m]
SD	Standard deviation of the mass increase among the 25 Petri dishes	[g]
CV	Coefficient of variation (SD / Average)	[-]

1. Introduction

Since the outbreak of the novel coronavirus disease 2019 (COVID-19), the critical role of indoor airflow control has become widely recognized [1–3]. In medical facilities where the risk of exposure to infectious patients is high, advanced and costly ventilation systems are required in specific areas, such as protective isolation units or airborne infection isolation rooms (AIIRs) [4,5]. The essential requirement for preventing airborne transmission is to ensure an adequate ventilation volume per person [6–8]. In addition, from the perspective of reducing the exposure risk of exhaled air from infected patients, displacement ventilation (DV) or floor-supply displacement ventilation (FSDV) is more appropriate than the traditional circular ceiling diffuser (CCD), in which exhaled air tends to be thoroughly mixed within the room [9–11]. DV is a system where fresh air is supplied from the floor or lower wall surfaces and flows upward with the human thermal plume, thereby exhausting exhaled air and body odors (bioeffluents) directly without mixing with the occupied zone air [12,13]. While careful operation is necessary in DV because insufficient ventilation volume can lower the concentration interface height and increase exposure in the breathing zone [14,15], several studies have shown that DV can effectively reduce infection risk when proper ventilation is maintained [16,17].

Among underfloor air distribution (UFAD) systems, the swirling flow-type floor diffuser (SFD) creates a highly mixed flow near the diffuser [18,19], whereas the horizontal flow-type floor diffuser (HFD) provides performance closer to displacement ventilation, contributing to infection risk reduction [17]. FSDV is a variant of UFAD, in which air is supplied from an underfloor plenum and evenly distributed across the entire floor surface through perforated panels and air-permeable carpet. With its large supply area, FSDV provides the lowest supply air velocity among various ventilation methods at equal total ventilation volume, thereby reducing the risk of local airflow drafts, although thermal drafts may still develop due to vertical stratification [19,20]. The authors' studies have demonstrated its superior performance in preventing airborne transmission [11,17,20]. Although its application is undesirable in rooms where liquids are likely to spill (e.g., operating rooms), the use of FSDV should be considered in protective isolation spaces, such as protective isolation rooms and airborne infection isolation rooms (AIIRs). However, FSDV has not been widely implemented because of cost considerations, thermal draft risks, and concerns about particle resuspension, despite the lack of empirical data under such conditions. Therefore, the purpose of this study is to quantitatively evaluate particle resuspension phenomena under FSDV conditions.

Numerous studies related to particle resuspension have been reported, including those investigating microscopic mechanisms such as aerodynamic, adhesion, and electrostatic forces, as well as those focusing on resuspension induced by actual human activities or their mechanical simulations [21–25]. Many of these studies have been conducted using experimental chambers, field measurements in offices and residences, or computational fluid dynamics (CFD). Field measurements in offices and residences have provided significant findings, such as locations where resuspension occasionally occurs or the floor loading mass of deposited particles, which can also inform chamber experimental conditions [26–28]. Other field measurements indicate that outdoor air is the primary source of fine particles (< 2 μm), while resuspension caused by human activity is the main source of larger particles (2–10 μm), despite the presence of filtration equipment [29–31]. Chamber studies have primarily examined parameters such as carpet material, relative humidity, and walking intensity. Although some opposite results exist across studies [32,33], the overall trend is that resuspension is higher on carpets than on hard tiles and increases when the humidity is lower [34–37]. Not only walking behavior, but other studies have also focused on the resuspension caused by infant crawling, showing that exposure for infants' breathing zone is significantly higher compared with adults, highlighting its importance as a research topic [38,39].

Other studies focusing on microscopic mechanisms have investigated the influence of particle and surface types, particle size, and deposition structure, revealing that resuspension behavior differs substantially between single-layer and multilayer deposition [24,40,41]. However, most of these studies were conducted under ceiling supply conditions or in small-scale wind tunnels, focusing on horizontal airflow or vibration-induced resuspension. Only a few studies have explored upward airflow conditions similar to FSDV, making experimental data under such conditions particularly valuable. For example, Kiyosuke et al. [42] compared airflow patterns among different ventilation methods and reported possible resuspension under FSDV during walking; however, their findings mainly described temporal concentration responses and did not provide quantitative indicators such as resuspension rate or fraction.

Based on these findings, this study focuses on the airflow-induced particle resuspension under FSDV conditions without human walking, as a preliminary step before conducting walking experiments in future

research. Furthermore, as previous studies suggested, resuspension is likely influenced by both aerodynamic drag forces and adhesive forces that are affected by relative humidity [43,44]. Therefore, experiments are conducted using humidity and supply air velocity as parameters under FSDV conditions (Fig. 1a). For comparison, additional experiments are performed under CCD conditions with traditional ceiling diffusers (commonly referred to as Anemostat diffusers) by varying supply air velocity at 50% relative humidity (Fig. 1b).

The objective of this study is to quantitatively evaluate airflow-induced particle resuspension under FSDV conditions and to identify its key influencing factors. Specifically, experiments were conducted with humidity and velocity as parameters, and the results were compared with those obtained under CCD conditions.

2. Methodology

2.1. Experimental procedures and facilities

The layout of the laboratory and its surrounding facilities is shown in Fig. 2. Experiments were conducted in a cleanroom chamber (hereafter referred to as the test chamber) owned by the University of Osaka. Supply air was introduced through a HEPA filter, and the system used 100% outdoor air without recirculation. The temperature was controllable, but humidity control was not available. The ventilation method could be switched between floor-supply displacement ventilation (FSDV) and circular ceiling diffuser (CCD) by changing the connection of the supply duct (Fig. 2). The ceiling diffuser (KUKEN Kogyo, C2 type, 200 mm φ) was operated in a heating-mode configuration, which provides a more vertical jet compared with the cooling setup, to simulate a more conservative (i.e., higher) resuspension scenario.

The ventilation rate was adjustable from 120 to 1000 m^3/h (corresponding to 6–50 air changes per hour). Both the supply and exhaust systems were equipped with constant air volume (CAV) units rated at 1000 m^3/h and 990 m^3/h, respectively, and were designed to maintain the test chamber at a slightly positive pressure, thereby preventing outdoor air infiltration. Because the supply and exhaust flow rates were not identical, the ventilation rate was adjusted based on the mass balance of CO_2 gas released into the exhaust duct. Therefore, in this study, the ventilation rate is defined as the exhaust airflow rate (Q_e).

A plan view and a cross-sectional view of the chamber are shown in Figs. 3a and 3b, respectively. The chamber floor was covered with 40 detachable air-permeable carpet tiles (each 500 mm × 500 mm). As illustrated in Fig. 3b, supply air entered the underfloor plenum and was uniformly distributed into the room through perforated metal panels and the air-permeable carpet layer. The carpet consisted of alternating high- and low-loop piles, with a Nylon 6 surface and a backing composed of glass fiber and polyester nonwoven fabric (Fig. 3c). The total air-supply area was 7 m^2, defined by the perforated panel region indicated in Fig. 3a.

Note that, in the absence of internal heat sources, the airflow pattern of FSDV resembled a piston-like flow from bottom to top, rather than the conventional displacement ventilation pattern.

The experimental procedure was as follows:

1. One gram of test particles was uniformly distributed on a single carpet tile in the entrance hall.
2. The particle-loaded carpet was transferred into the test chamber (Fig. 3a), and placement was completed within 2 minutes by the operator to minimize unintended particle dispersion. The ventilation system (FSDV or CCD) was operated continuously throughout the experiment, including before operator entry.
3. The carpet was then exposed to airflow for a specified duration (t_e; Table 1), during which temporal variations in particle number concentration were continuously monitored using four handheld particle counters (Model 3889, Kanomax Japan Inc.) installed at fixed positions, as shown in Fig. 3b.

Particle counters were installed at heights of 150, 1100, and 1700 mm above the floor, as shown in Fig. 3b. The 150 mm height was selected as the lowest feasible measurement position given the experimental setup and was used for resuspension rate calculations under FSDV, where particle concentrations were expected to be highest near the carpet surface. The additional heights of 1100 and 1700 mm correspond to representative breathing-zone levels for seated and standing occupants, respectively, and were selected with reference to commonly used indoor environmental measurement guidelines (e.g., ISO 7726) [45].

Temperature and relative humidity were simultaneously measured at three locations: within the underfloor supply plenum (point *t*), inside the test chamber (point *s*), and in the entrance hall (point *e*), using a Vaisala HUMICAP® Handheld Humidity and Temperature Meter (Model MI70 with HMP75 probe) (Figs. 2 and 3b). The saturated vapor pressure was calculated using the Wexler–Hyland equation (Eq. (1)) [1]. Relative humidity was then calculated using Eq. (2), and absolute humidity was derived using Eq. (3).

$$ln e_s(T) = A_1/T + A_2 + A_3 T + A_4 T^2 + A_5 T^3 + A_6\ lnT \quad (1)$$

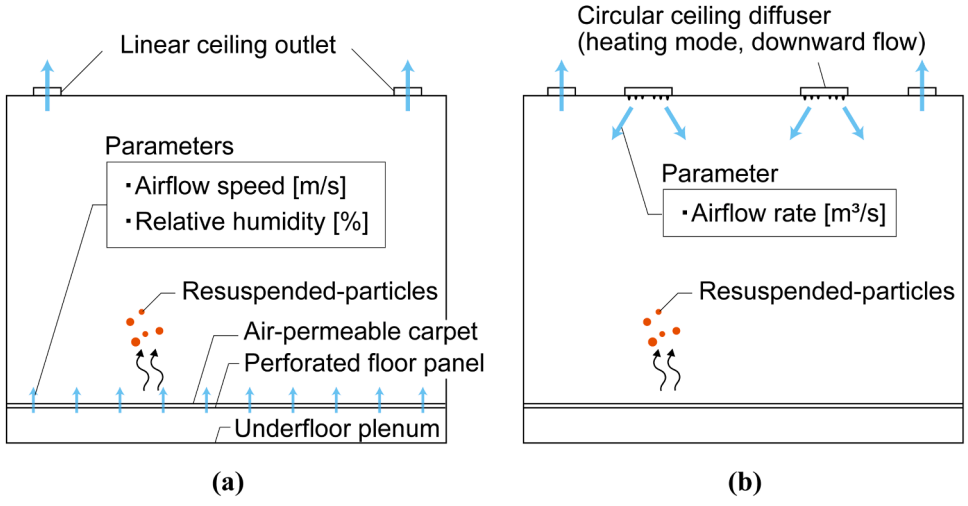

Fig. 1. Schematic cross-section and key parameters of this study. **(a)** Air supply method: floor-supply displacement ventilation (FSDV). **(b)** Air supply method: circular ceiling diffuser (CCD) as a comparison case.

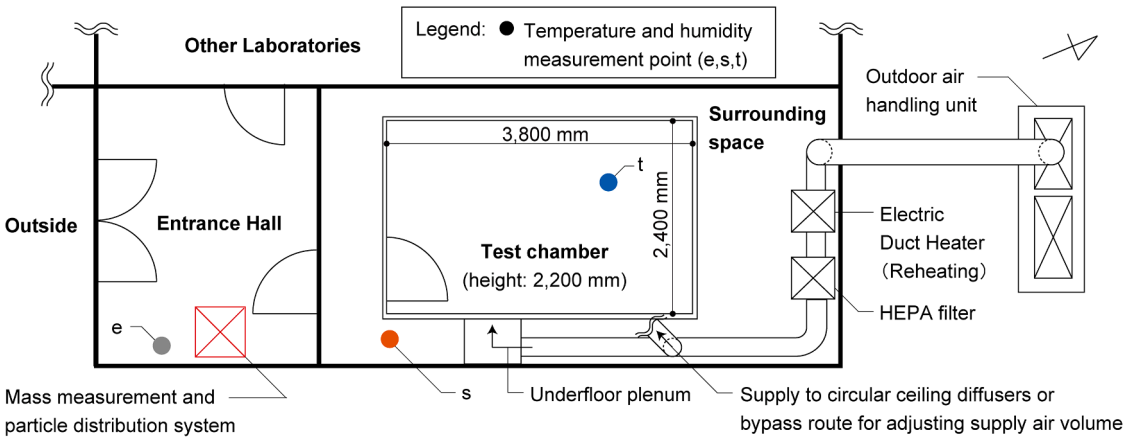

Fig. 2. Schematic layout of the test chamber and surrounding environment.

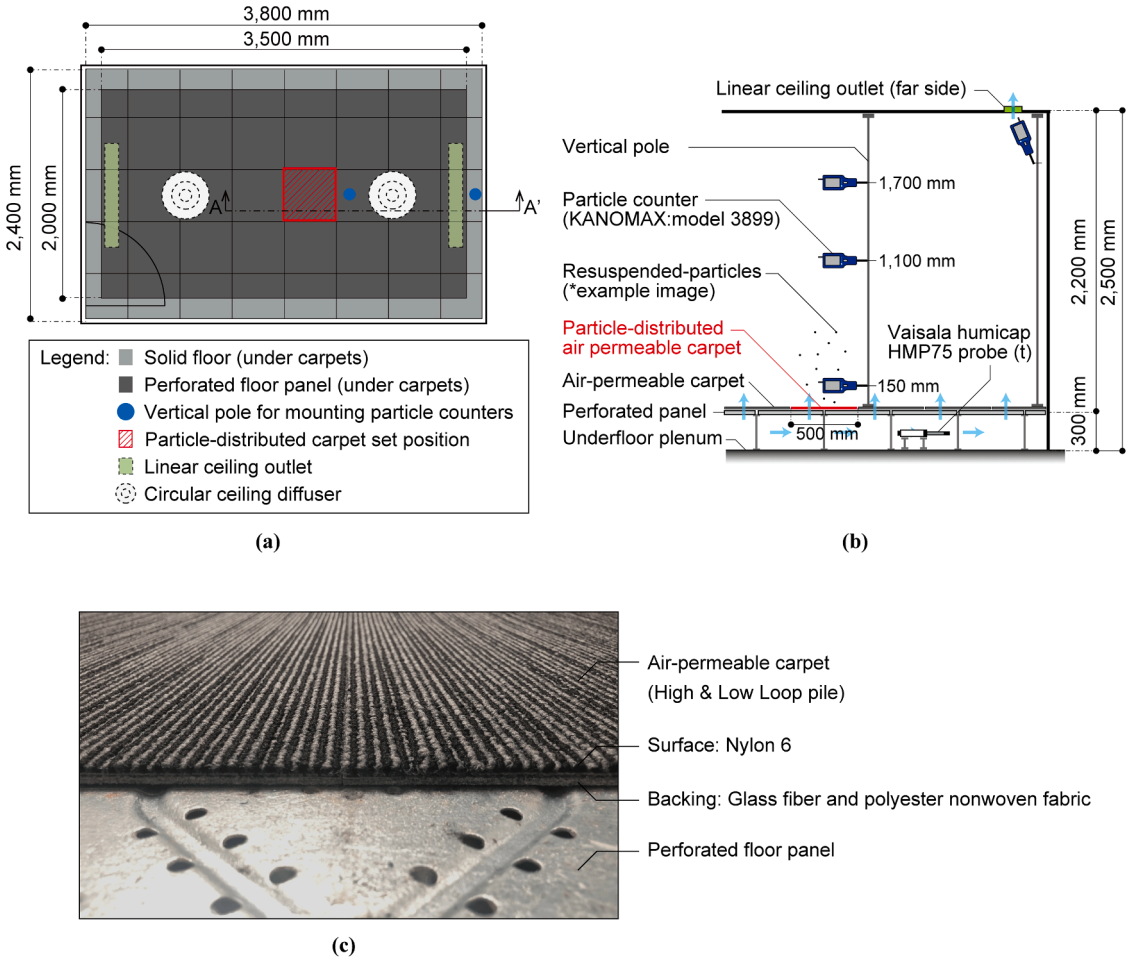

Fig. 3. Details of the test chamber. **(a)** Plan view of the test chamber. A linear ceiling outlet and a circular ceiling diffuser are on the ceiling, displayed in dotted lines. **(b)** Cross-sectional view of the test chamber along line A–A′ (particle concentration measurement points). **(c)** Photograph of the air-permeable carpet and perforated floor panel with annotated cross-sectional details.

$$e = RH * e_s(T)/100 \quad (2)$$

$$AH = (216.7 * e)/(T + 273.15) \quad (3)$$

where e_s (T) is the saturation vapor pressure [hPa], T is the dry-bulb temperature [K], A_1-A_6 is the empirical constants ($A_1 = -0.58002206\times10^{3}$, $A_2 = +0.13914993\times10^{1}$, $A_3 = -0.48640239\times10^{-1}$, $A_4 = +0.41764768\times10^{-4}$, $A_5 = -0.14452093\times10^{-7}$, $A_6 = +0.65459673$) (reported by Hyland and Wexler (1983) [1]), e is the water vapor pressure [hPa], RH is the relative humidity [%], and AH is the absolute humidity [g/m^3].

2.2. Particle dispersion on carpet

Details of the equipment used for mass measurement and particle

Table 1
Test names and details of experimental conditions.

Test name	v_f [m/s]	r_d [-]	$RH(t)$ [%]	Q_e [m^3/h]	A [h^{-1}]	τ_n [min]	t_e [min]	L_{total} [g] ([g/m^2])
FSDV_0.04_20	0.04	16	20	990	49.3	1.2	24.3	1.00 (4.00)
FSDV_0.04_50	0.04	16	20	990	49.3	1.2	24.3	1.00 (4.00)
FSDV_0.04_80	0.04	16	20	990	49.3	1.2	24.3	1.00 (4.00)
FSDV_0.03_20	0.03	9	50	750	37.4	1.6	32.1	1.00 (4.00)
FSDV_0.03_50	0.03	9	50	750	37.4	1.6	32.1	1.00 (4.00)
FSDV_0.03_80	0.03	9	50	750	37.4	1.6	32.1	1.00 (4.00)
FSDV_0.01_20	0.01	1	80	250	12.5	4.8	96.3	1.00 (4.00)
FSDV_0.01_50	0.01	1	80	250	12.5	4.8	96.3	1.00 (4.00)
FSDV_0.01_80	0.01	1	80	250	12.5	4.8	96.3	1.00 (4.00)
CCD_850_50	-	-	50	850	42.4	1.4	28.3	1.00 (4.00)
CCD_750_50	-	-	50	750	37.4	1.6	32.1	1.00 (4.00)
CCD_250_50	-	-	50	250	12.5	4.8	96.3	1.00 (4.00)
FSDV_0.04_20_no	0.04	16	20	990	49.3	1.2	24.3	-
CCD_850_50_no	-	-	50	850	42.4	1.4	28.3	-

v_f: Area-averaged supply air velocity over flow-through panels [m/s]; r_d: Dynamic pressure ratio relative to v_f =0.010 m/s [-]; RH(t): Relative humidity in test chamber [%]; Q_e: Exhaust airflow rate [m^3/h]; A: Air change rate [h^{-1}]; τ_n: Nominal time constant [min]; t_e: Duration of carpet exposure to airflow [min]; L_{total}: Total applied mass of particles on the carpet [g].

dispersion, installed in the entrance hall, are shown in Fig. 4. A tare plate and a carpet support made of foamed polystyrene were placed on a tuning fork-type electronic balance (RJ-620, Shinko Denshi Co., Ltd.; minimum resolution: 0.001 g). To minimize the influence of ambient airflow, the entire apparatus was enclosed within a wind shield constructed from steel angles and vinyl sheets. A commercially available cosmetic powder sprayer was employed for particle application.

To ensure uniform spreading, the upper surface of the wind shield was divided into 16 equal sections, and particles were applied sequentially from each division point (Fig. 5a). The uniformity of particle deposition was confirmed in a separate validation experiment, showing that the standard deviation among 25 divided surface sections was within 1% (Appendix A).

An image of the carpet after the application of 1 g of powder is shown in Fig. 5b. The applied mass—equivalent to 4 g/m^2—was determined with reference to previous studies: 20 g/m^2 reported by J. Qian et al.[37] and 0.221–2.971 g/m^2 reported by J. Rostami et al.[46], both of which used Arizona Test Dust (ATD A1). For the test particles, a commercially available pharmaceutical powder, Ryukakusan (Ryukakusan Co., Ltd.), was selected to ensure operator safety. Ryukakusan is a finely ground mixture of herbal ingredients, most of which are insoluble in water. According to Y. Takeuchi et al. [47], its density is 2.80 g/cm^3, and the volume-based median diameter (D_{50}) is 7.7 μm. These values are comparable to—but slightly larger than— those of Arizona Test Dust A1, which has a density of 2.65 g/cm^3 and a mass-based median diameter (D_{50}) of 4.3 μm and has been widely used in previous studies [22]. To further confirm the suitability of Ryukakusan as a surrogate test particle, comparative experiments were conducted using Arizona Test Dust A1 (ATD A1) under identical FSDV conditions. As shown in Appendix C, both particles exhibited resuspension rates of the same order of magnitude across the examined particle size ranges.

The surface of the air-permeable carpet consisted of a nylon 6 loop pile, while the backing layer was composed of glass fiber and polyester nonwoven fabric (Fig. 3c). Because nylon 6 is hygroscopic, its mass can vary depending on the ambient moisture content. Consequently, it is difficult to determine whether changes in carpet mass observed during particle application are attributable to moisture absorption or desorption, or to the adhesion of particles themselves. On average, approximately 10 minutes were required to apply 1 g of powder onto a carpet tile. Therefore, it was assumed that the rate of moisture absorption during spraying was equivalent to that occurring during the 10 minutes immediately preceding spraying.

To validate this assumption, mass changes were measured for ten individual carpet samples over a continuous 20-minute period (Fig. 6). The mean absolute mass change over a 10-minute interval was 2.46 mg, with a standard deviation of 1.57 mg. This variation corresponds to less than 0.25% of the target application mass (1 g). Using this procedure, a particle application (adhesion) of 1.000 ± 0.020 g was consistently achieved under all experimental conditions summarized in Table B-1.

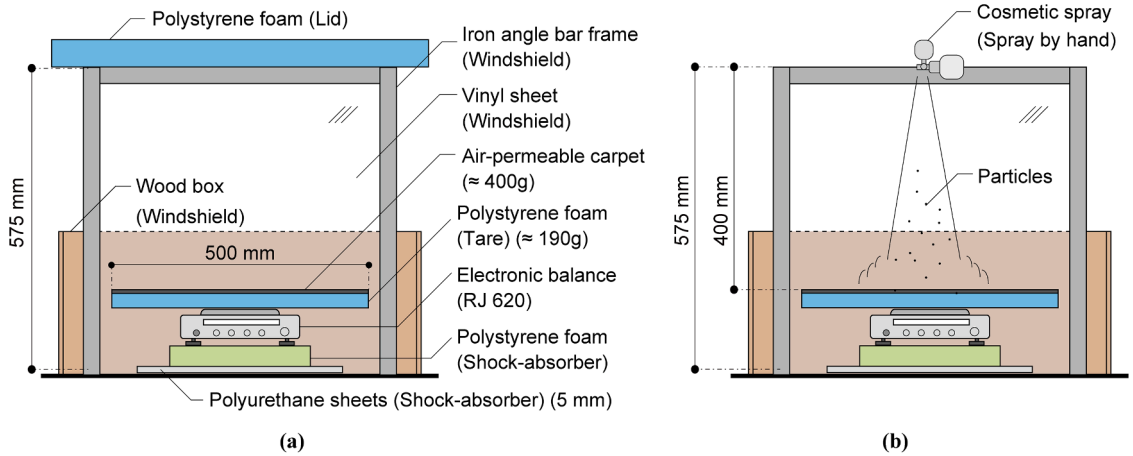

Fig. 4. Mass measurement and particle distribution system installed in the entrance hall shown in Fig. 2. **(a)** Setup for carpet mass measurement. **(b)** Particle distribution process on the carpet.

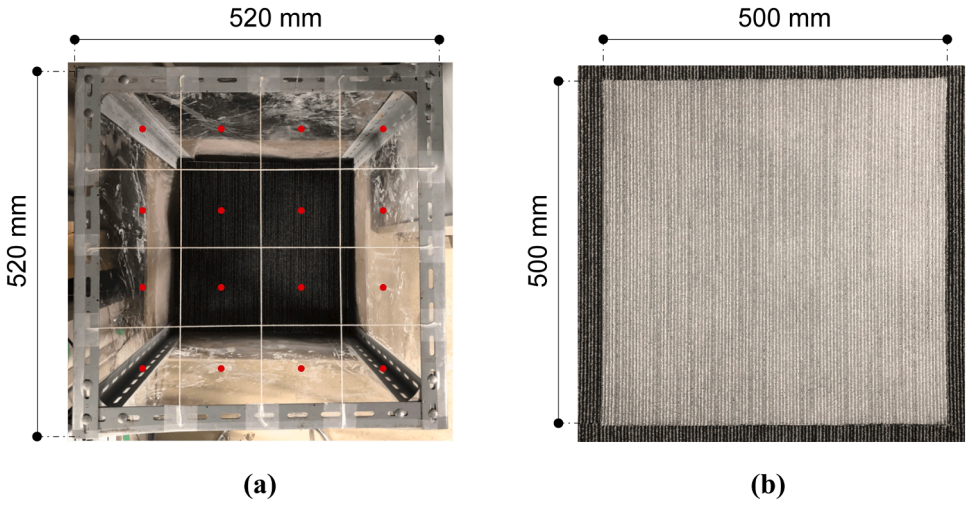

Fig. 5. Photographs of particle dispersion. **(a)** Top view of particle distribution points. **(b)** Carpet surface after particle distribution (≈ 1.0 g).

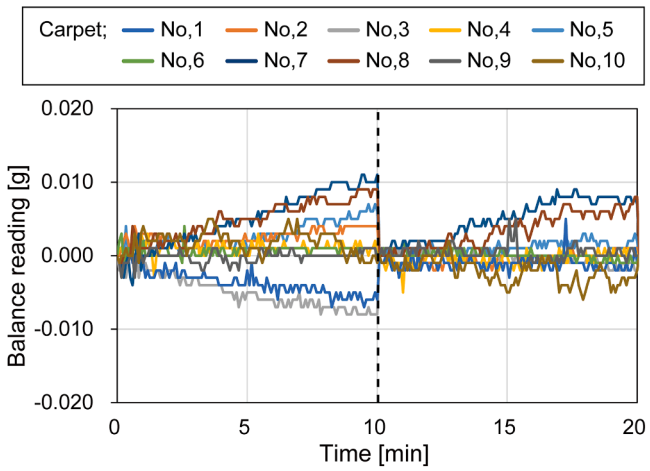

Fig. 6. Mass change of 10 different carpets (Carpet No. 1–10) over 20 minutes (normalized to zero at 10 minutes, including tare weight).

2.3. Parameters and experimental cases

The key parameters influencing resuspension were the floor supply air velocity (v_f) and the relative humidity (RH) of the supply airflow under FSDV conditions. Experiments under CCD conditions were also conducted for comparison. Table 1 summarizes the experimental cases, including their naming conventions and configurations. Each test name consisted of the ventilation method, the floor supply air velocity in FSDV (or the ventilation volume in CCD), and the relative humidity. Table 1 also presents the relationship between the area-averaged floor supply air velocity in FSDV and other relevant parameters. Here, v_f is defined as the supply airflow rate divided by the total area of the flow-through panels shown in Fig. 3a.

For comparison, control cases were established for FSDV at v_f = 0.040 m/s and RH = 20%, and for CCD at 850 m^3/h and RH = 50%, both without any particles applied to the carpet (non-seeded). In these control cases (FSDV_0.04_20_no and CCD_850_50_no), only carpet installation and operator entry/exit were performed. No internal heat sources were present in the chamber for any test condition.

The area-averaged floor supply air velocity in FSDV was tested at three levels—0.010, 0.030, and 0.040 m/s—selected such that the corresponding dynamic pressure ratios were approximately evenly spaced, with v_f = 0.010 m/s used as the reference condition, as shown in Table 1 (r_d). This design enables a systematic investigation of resuspension behavior under increasing aerodynamic forcing, considering that resuspension is governed by drag forces proportional to the dynamic pressure of supply airflow. Each v_f was adjusted by varying the total supply airflow rate. A supply velocity of 0.040 m/s corresponds to 50 air changes per hour (ACH), a level typically required in hospital cleanrooms [4]. A velocity of 0.010 m/s corresponds to 12.5 ACH, consistent with the HEAS-02-2022 recommendation of 12 ACH for Airborne Infection Isolation Rooms (AIIRs) [4]. According to the carpet manufacturer, the recommended operating range is below approximately 0.014 m/s; therefore, 0.010 m/s was selected to represent typical operating conditions. The selected RH levels (20%, 50%, and 80%) were determined based on both practical relevance and previous literature. For example, Qian et al. (2008) investigated resuspension at 30% and 50% RH and reported relatively limited differences, suggesting that a wider RH range is necessary to fully capture humidity effects [37]. Rosati et al. (2008) examined walking-induced resuspension at 20%, 40%, and 80% RH [46], while Tian et al. (2014) compared low (30–40%) and high (70–80%) RH ranges and reported that humidity effects may vary depending on carpet characteristics [48]. Considering these findings, the present study adopted a wide RH range (20%, 50%, and 80%) to systematically examine humidity-dependent resuspension behavior under FSDV airflow.

In CCD experiments, the supply airflow rate was varied as a parameter while maintaining RH = 50%. To match the flow condition corresponding to v_f = 0.040 m/s in FSDV, a flow rate of 990 m^3/h would have been required. However, due to limitations of the outdoor air handling unit fan, the maximum achievable rate was 850 m^3/h. The relative humidity of 50% was selected as a representative indoor environmental condition commonly adopted in office and healthcare facilities. Although lower humidity conditions (e.g., 20%) were examined under FSDV to evaluate resuspension under worst-case conditions, such low RH levels are uncommon in actual buildings. According to ANSI/ASHRAE/ASHE Standard 170, acceptable RH in healthcare spaces ranges from 20–60% [49], and CDC guidance recommends maintaining indoor RH below 60% [5]. Therefore, 50% RH lies near the midpoint of these recommended ranges and was adopted as a realistic reference condition for CCD experiments.

The experimental duration (t_e) was set to 20 times the nominal time constant for each condition. Relative humidity was controlled at three levels (20%, 50%, and 80%) using an outdoor air conditioner and an electric duct reheater (Fig. 2). The average relative humidity in the underfloor supply plenum (Fig. 3b) was maintained within ±7% of the target value under all conditions, as summarized in Table B-1. The supply air temperatures during the measurement ranged from 17°C to 34°C (Table B-1).

2.4. Calculation of resuspension rate

The resuspension rate (coefficient), r [h^{-1}], is defined as the fraction of particles deposited on the floor surface that are resuspended per unit time. The calculation procedure is summarized in Eqs. 4–10 [21,22].

2.4.1. Definition of the resuspension rate

First, Eq. (4) defines the resuspension rate r_j as the ratio of the resuspended mass per unit time (R_j) to the deposited mass (L_j) for each particle size range j:

$$r_j = R_j / L_j \tag{4}$$

2.4.2. Calculation of R_j under FSDV conditions

Under FSDV conditions, the resuspended mass $R_{j,\ FSDV}$ is calculated using Eq. (5). A conversion factor (α) is introduced to convert the measured concentration at 150 mm above the carpet into the total resuspended amount from the entire carpet area:

$$R_{j,\ FSDV} = \frac{\alpha}{n\Delta t} \sum_{i=1}^{n} \left(N'_{pc,i,j} V_j \rho \right) \tag{5}$$

whwer α is the conversion factor accounting for the total resuspension amount (210.2, 157.7, and 52.6 for $v_f = 0.040$, 0.030, and 0.010 m/s) [–], n is the total number of time steps (total number of data points) [-], Δt is the duration of each time step (constant within each test case; 6 s for flow rates of 1000, 850, and 750 m^3/h, and 12 s for 250 m^3/h) [s], $N'_{pc,i,j}$ is the number of particles measured at time step i for size range j, with the 10-minute average value prior to operator entry subtracted [-], ρ_p is the Particle density (2.83 for Ryukakusan [47]) [g/m^3], and V_j is the representative particle volume for size range j [m^3].

The conversion factor α is defined as the ratio of the airflow volume per carpet tile (Q_{ca}) to the suction flow rate of the particle counter (q_{pc}), as shown in Eq. (6):

$$\alpha = Q_{ca} / q_{pc} \tag{6}$$

wherw Q_{ca} is the airflow volume per 500×500 mm air-permeable carpet tile [m^3/h], and q_{pc} is the suction flow rate of particle counter (0.170) [m^3/h].

The calculated α values were 210.2, 157.7, and 52.6 for $v_f = 0.040$, 0.030, and 0.010 m/s, respectively. This assumption is considered valid near the carpet surface, but not at greater heights where diffusion becomes dominant. Accordingly, the resuspension rate r was calculated only from the particle counter positioned 150 mm above the floor.

2.4.3. Background correction and observation period

To eliminate the influence of background particles, the 10-minute average concentration measured prior to operator entry was subtracted from the measured data using Eq. (7):

$$N'_{pc,i,j} = N_{pc,i,j} - \overline{N_{pcb,j}} \tag{7}$$

whwer $N_{pc,i,j}$ is the number of particles measured at time step i for size range j [-], and $\overline{N_{pcb,j}}$ is the average number of particles measured during the 10 minutes before operator entry, for size range j [-].

The total observation time ($n\Delta t$) corresponds to the period between 10 and 20 nominal time constants after the operator's entry, as shown in Eq. (8):

$$n\Delta t = 10 \frac{V_r}{Q_e} \tag{8}$$

where V_r is the room volume (20.06) [m^3], and Q_e is the exhaust airflow rate [m^3/h].

2.4.4. Calculation of R_j under CCD conditions

Under CCD conditions, the resuspended particles from the 500 × 500 mm carpet tile were assumed to disperse uniformly throughout the chamber. The total resuspended mass was thus estimated by multiplying the particle mass concentration by the chamber volume, as expressed in Eq. (9):

$$R_{j,CCD} = \frac{V_r}{n\Delta t} \sum_{i=1}^{n} \left(\frac{N'_{pc,i,j} V_j \rho_p}{q_{pc}\ \Delta t} \right) \tag{9}$$

To verify the assumption of complete mixing, results obtained from both the 150 mm height and the ceiling outlet were compared, confirming that the assumption was approximately valid (Figs. 10d and 10e).

2.4.5. Estimation of deposited mass L_k

The deposited mass L_j for each size range was estimated using Eq. (10):

$$L_j = L_{total} f_p \tag{10}$$

whwre L_{total} is the total applied mass of particles on the carpet (1.000 ± 0.003) [g], and f_p is the mass fraction of test particles in each particle size class [–]

The particle size distribution of Ryukakusan (f_p) was obtained from Y. Takeuchi et al. [47]. This distribution was obtained using a laser diffraction particle size analyzer (LDSA-2400A, originally developed by Tohnichi Computer Applications Co., Ltd.; now managed by MicrotracBEL Corp.). Based on the mass fraction of each particle size class (Table 2), L_j was determined by multiplying the total deposited mass (1.000 ± 0.030 g) by the corresponding fraction, assuming that the reported distribution also applied to particles deposited on the carpet surface.

3. Results

3.1. Time series of indoor particle concentration

Fig. 7 shows the time-series variation in particle number concentration by particle size at a height of 150 mm above the floor under no-particle conditions (FSDV_0.04_20_no, Fig. 7a; CCD_850_50_no, Fig. 7b). Fig. 8 presents the time-series variation in particle number concentration by particle size measured by the four particle counters shown in Fig. 3, under the FSDV_0.04_20 condition. In Figs. 7–9, the average background concentration for each particle size class during the 10 minutes before operator entry was subtracted from the measured data (Eq. (7)), ensuring consistent data processing across all test conditions. As shown in Figs. 8 and 9, after approximately 10 nominal time constants following carpet placement, the concentration decayed to near-background levels, and resuspension-related peaks became clearly identifiable.

Comparing Figs. 7a and 7b, particle concentrations exhibited a temporary increase immediately after operator intrusion, but the subsequent decay patterns showed no substantial difference between FSDV and CCD. Even when no particles were applied to the carpet, a slight particle concentration was observed—approximately 2.5 × 10^4 m^{-3} in the 0.3–0.5 μm size range.

Comparing Fig. 7a and Fig. 8d, numerous sharp peaks in particle concentration were observed at 150 mm above the floor in Fig. 8d, indicating that particle resuspension occurred. Although 0.3–0.5 μm

Table 2
Mass ratio of test particles (Ryukakusan) in each particle size class (f_p), estimated from Y. Takeuchi et al. [47].

0.3-0.5 μm	0.5-1.0 μm	1.0-3.0 μm	3.0-5.0 μm	5.0-10 μm	10- μm
0.01	0.01	0.09	0.19	0.40	0.30

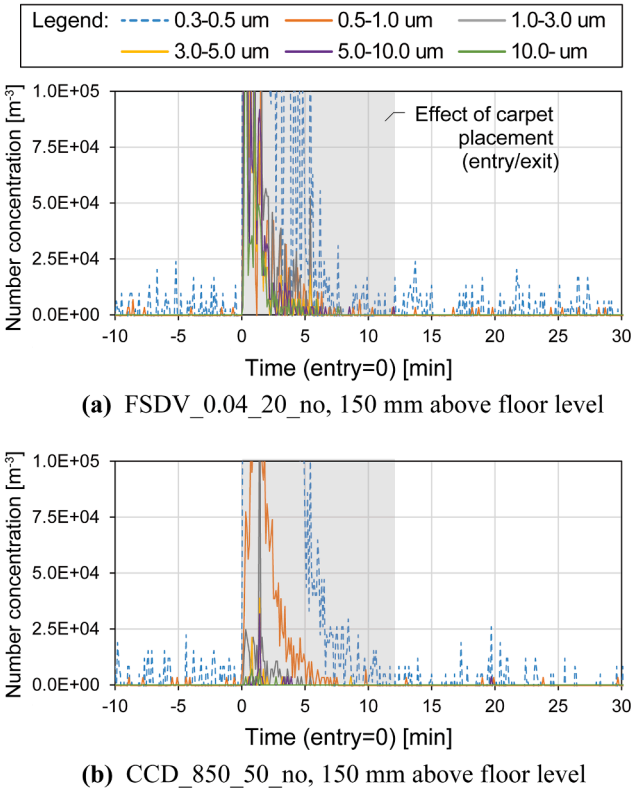

Fig. 7. Time series of size-resolved particle number concentrations at 150 mm above the floor. **(a)** FSDV_0.04_20_no. **(b)** CCD_0.04_20_no.

particles were dominant, distinct peaks also appeared in the 5–10 μm and >10 μm ranges, whereas no such peaks were present in Fig. 7a. In contrast, the frequency and amplitude of peaks decreased with increasing height, as shown in Figs. 8c (1100 mm), 8b (1700 mm), and 8a (exhaust concentration), confirming that resuspension effects were most pronounced near the floor surface.

Fig. 9 displays the time series of size-resolved particle number concentrations measured 150 mm above the floor under all experimental conditions. To enable comparison across different ventilation volumes, the horizontal axis was normalized by the nominal time constant for each condition. The interval corresponding to 10–20 normalized ventilation times was used for calculating the resuspension rate.

Among all conditions, resuspension was most pronounced under FSDV_0.04_20, as shown in Fig. 9a. The influence of relative humidity is also evident: resuspension was markedly lower under the FSDV_0.04_80 condition. In contrast, under the $v_f = 0.010$ m/s condition (Figs. 9g–i), overall resuspension levels were low, and the impact of humidity appeared minimal.

Under CCD conditions, humidity was kept constant while the airflow rate was varied. At 850 m^3/h and 750 m^3/h, several peaks indicating measurable resuspension were observed, whereas at 250 m^3/h, the number and amplitude of peaks decreased substantially. Compared with FSDV, resuspension peaks under CCD were less frequent but broader, and the average particle concentration was higher, likely because resuspended particles dispersed horizontally before diffusing throughout the chamber.

3.2. Resuspension rate

Fig. 10 shows the calculated resuspension rates [h^{-1}] for each condition, plotted as a function of particle size. Results under FSDV conditions are presented in Figs. 10a–c, while those under CCD conditions are shown in Figs. 10d and 10e. To eliminate the influence of background

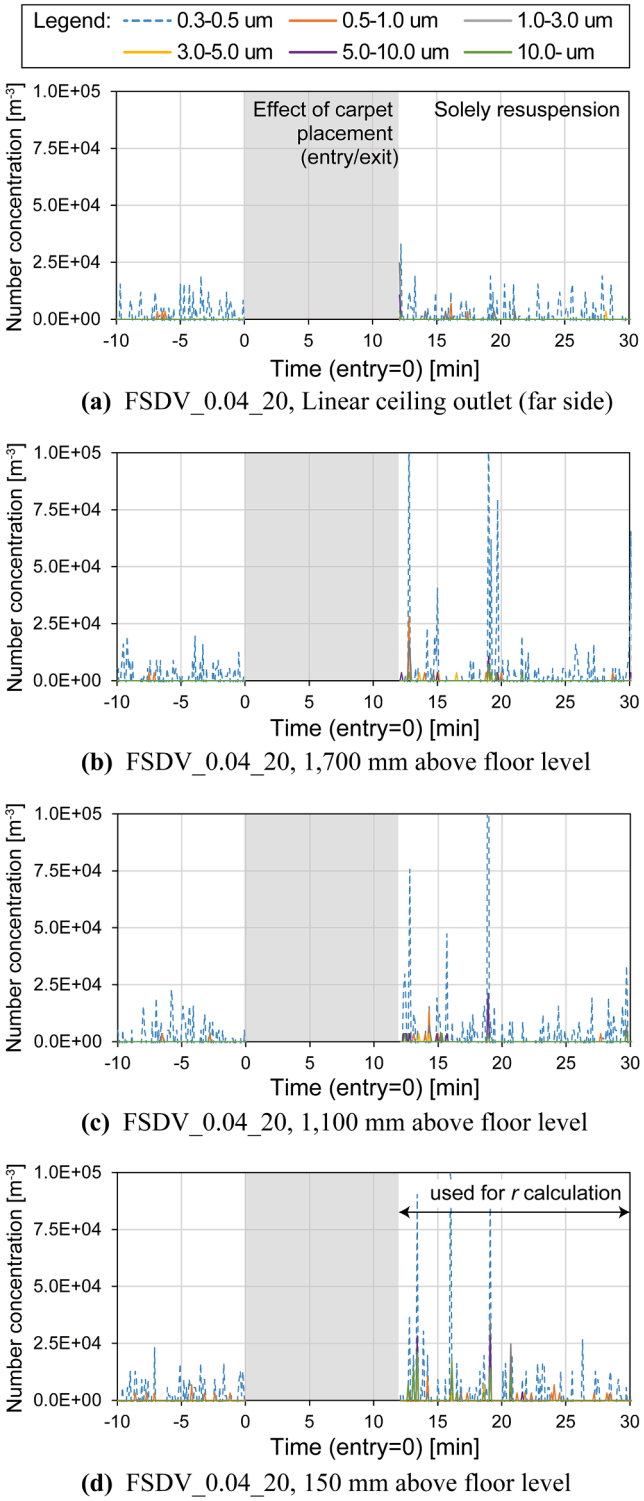

Fig. 8. Time series of size-resolved particle number concentrations under the FSDV_0.04_20 condition. Measurement locations of particle counters are shown in Fig. 3b. **(a)** Linear ceiling outlet, located far from the entrance door. **(b)** 1700 mm above floor level. **(c)** 1100 mm above floor level. **(d)** 150 mm above floor level. The shaded region indicates the period excluded from a resuspension rate calculation.

concentration, the 10-minute average concentration measured prior to operator entry was subtracted for each particle size range (Eq. (7)). As a result, some negative or zero values were obtained, which cannot be represented on a logarithmic scale; therefore, a "0 region" was added

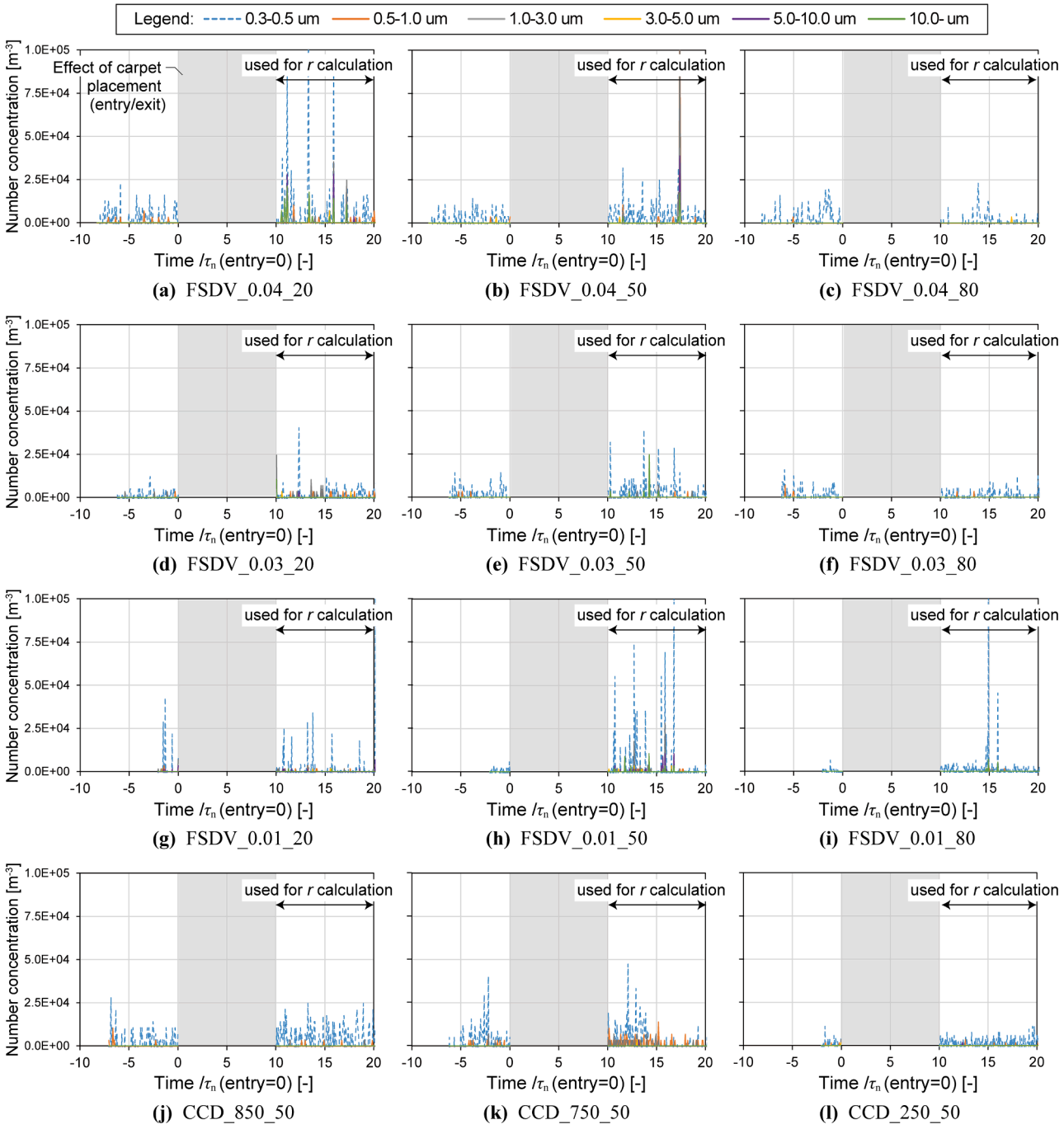

Fig. 9. Time series of size-resolved particle number concentrations at 150 mm above the floor. The horizontal axis represents time relative to the operator's entry (entry = 0), normalized by the nominal time constant. Results of all experimental cases are shown in **(a)–(l)**. The shaded region indicates the period excluded from a resuspension rate calculation.

below the main plot to display these data points. For the FSDV_0.04_50 case in Fig. 10a, error bars represent ±1 standard deviation obtained from five repeated experiments (n = 5), indicating measurement variability under low-resuspension conditions, as shown in Appendix C.

Comparing Figs. 10a–c, it is evident that the resuspension rate decreases with decreasing floor supply air velocity. Conversely, when comparing relative humidity at the same air velocity, the influence of humidity is more pronounced at 0.040 m/s (Fig. 10a), while its effect is minimal at 0.010 m/s (Fig. 10c). Regarding particle size, particles in the 5–10 μm and ≥10 μm ranges exhibited relatively higher resuspension rates at 150 mm above the floor. However, there remain significant uncertainties concerning the behavior of particles after resuspension under FSDV conditions.

Under CCD conditions, assuming complete mixing, the total resuspended mass was calculated by multiplying the particle number concentration by the chamber volume. To verify this assumption, the resuspension rate was calculated separately using data from particle counters installed at 150 mm above the floor and below the linear ceiling outlet. As shown in Figs. 10d and 10e, the results from the two measurement heights exhibited no substantial differences in either order of magnitude or overall trend, thereby confirming the validity of the complete mixing assumption.

The resuspension rates under CCD conditions ranged approximately from 10^{-5} to 10^{-3} h^{-1}, generally higher than those observed under FSDV

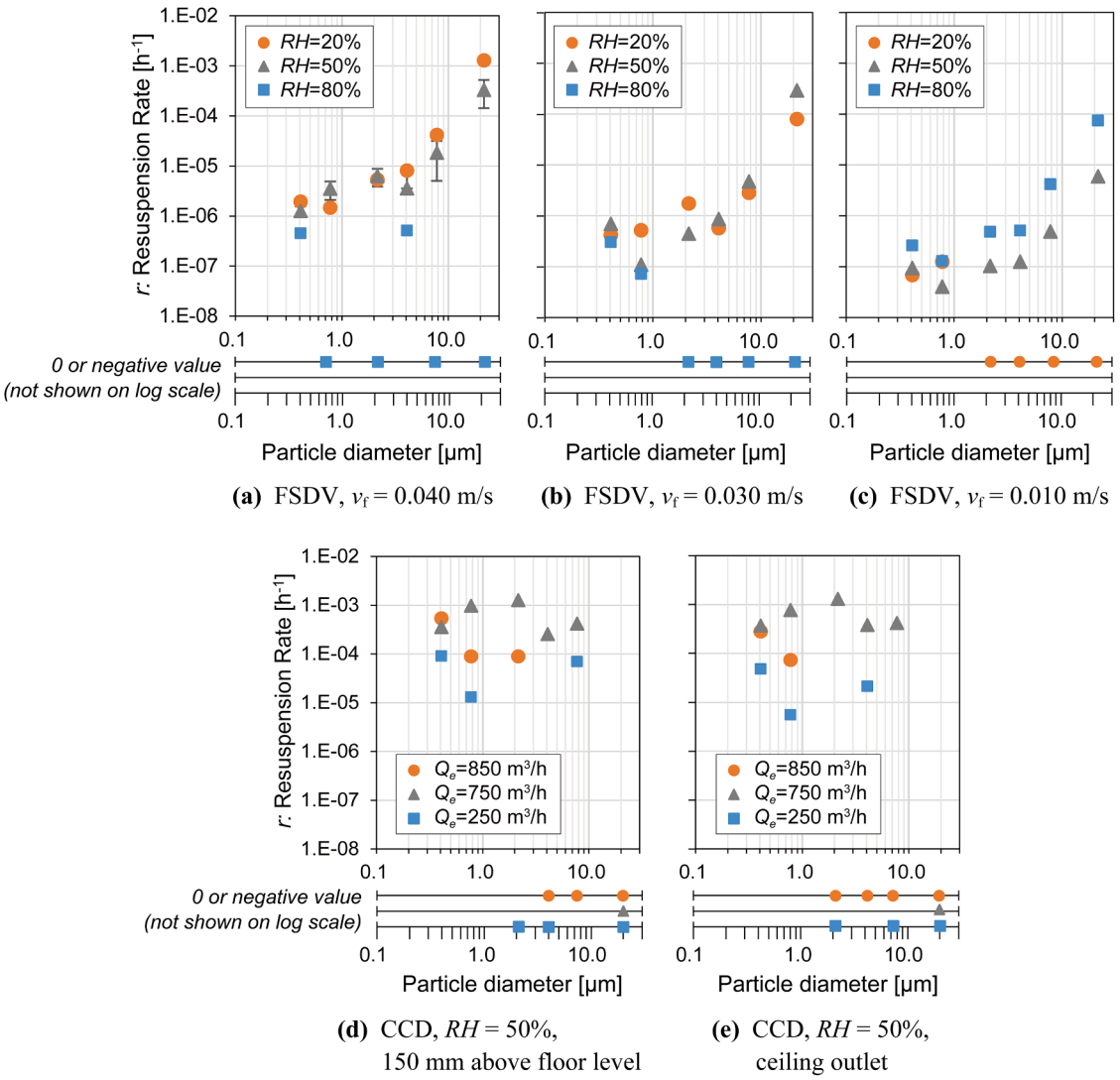

Fig. 10. Size-resolved resuspension rates (r, [h^{-1}]) under each experimental condition (both axes in logarithmic scale). **(a–c)** FSDV cases with floor supply velocities (v_f) of 0.040, 0.030, and 0.010 m/s, respectively, at relative humidities (*RH*) of 20%, 50%, and 80%, measured 150 mm above the floor. **(d, e)** CCD cases at *RH* = 50%, measured 150 mm above the floor **(d)** and at the ceiling outlet **(e)**. For CCD, ventilation rates Q_e were 850, 750, and 250 m^3/h. The lower panels indicate data points with zero or negative values (not shown on a log scale).

conditions. When examined by particle size, for particles larger than 3 μm, several size classes yielded zero or negative values, and for those larger than 10 μm, the resuspension rate was zero at 150 mm above the floor for all ventilation rates. The maximum achievable CCD airflow rate was 850 m^3/h due to fan capacity limitations, although 990 m^3/h would be required to match $v_f = 0.040$ m/s in FSDV. As shown in Figs. 10d and 10e, CCD resuspension rates did not vary monotonically with airflow rate and were strongly influenced by intermittently detected resuspension peaks. Therefore, the 14% difference between 850 and 990 m^3/h is unlikely to change the qualitative conclusions of this study.

3.3. Close-up images of the carpet

The carpet fibers were imaged using a Phone Micro 5 microscope (APEXEL, MS200) at 200× magnification. The camera had a resolution of 12 MP (4032 × 3024 pixels). Close-up images are shown in Fig. 11. Image pairs (a) and (a′) correspond to the same locations, respectively. Images (a)–(e) were taken before airflow exposure, whereas (a′)–(e′) were taken after 30 minutes of airflow exposure. These observations were conducted under the conditions of $v_f = 0.040$ m/s and 50% relative humidity.

The air-permeable carpet was installed over a metal panel with evenly spaced perforations, each 6 mm in diameter, and the photographed fibers were located directly above these holes. Each perforated panel contained 328 holes (6 mm diameter), giving an open area ratio of approximately 4.5%. From the 160× images, regions showing visible changes were selected and further magnified to 800× for detailed comparison.

The pre-exposure images (Fig. 11a–e) show numerous particle aggregates larger than 10 μm. Approximately 50% of Ryukakusan particles have a volume-based diameter of ≤7.7 μm [47]; however, because of image resolution limitations, the presence and condition of submicron particles could not be clearly evaluated, making it difficult to determine the adhesion ratio for each particle size. The large aggregates observed may have either been deposited as clusters during the spraying process using the cosmetic powder sprayer or coalesced on the fiber surface after deposition.

When comparing the close-up images taken after airflow exposure (Fig. 11a′–e′) with those taken before exposure (Fig. 11a–e), several particles in the 50–100 μm range appear to have moved or disappeared from the field of view. This phenomenon is likely attributed to the increase in aerodynamic drag with particle size, while the contact area

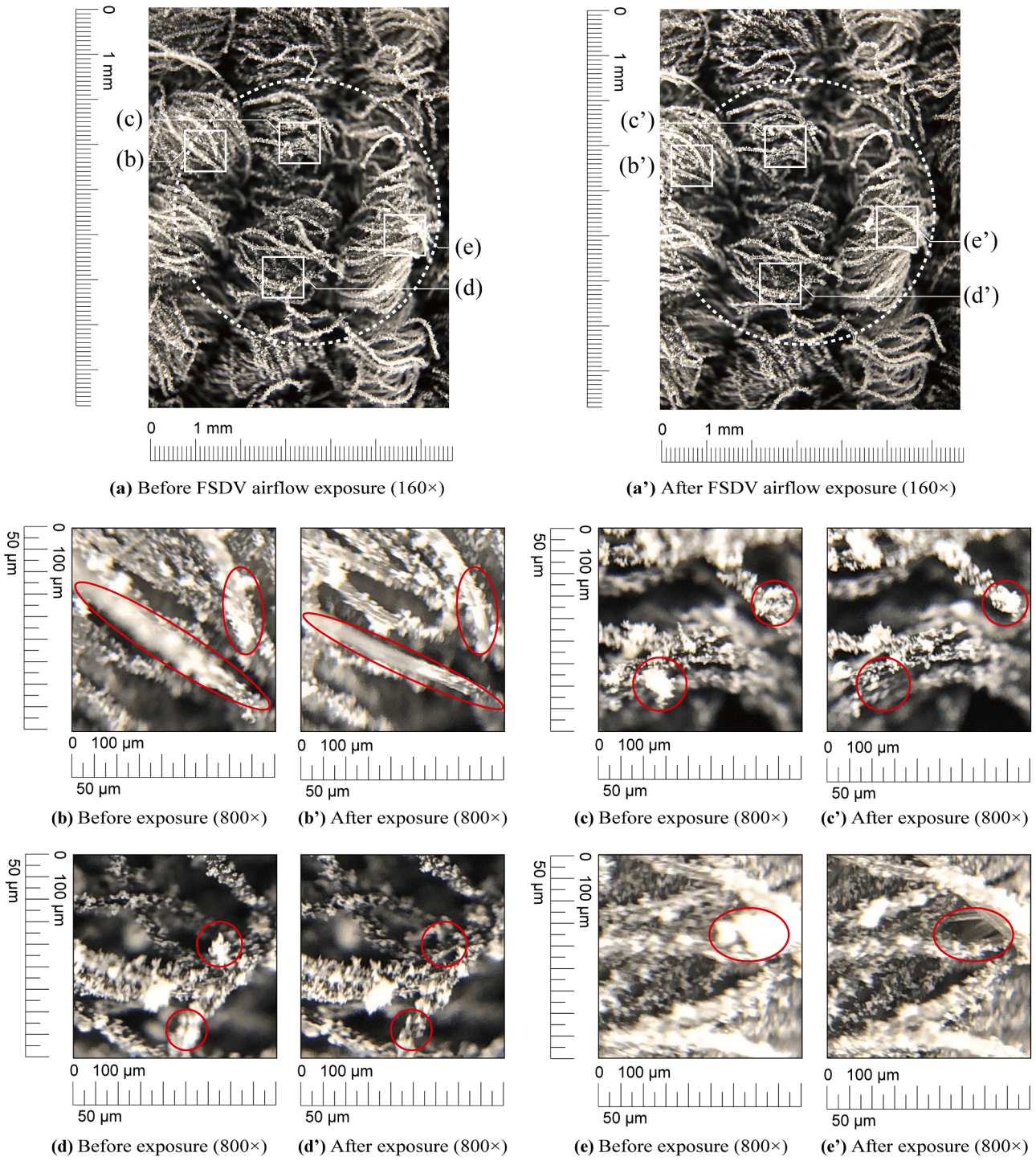

Fig. 11. Close-up images of the carpet in Case FSDV_0.04_50. **(a)** Before airflow exposure (magnification: 160×); **(a′)** After 30 min of airflow exposure (magnification: 160×). White dotted circles in **(a)** and **(a′)** indicate approximate positions of the 6 mm diameter punched metal holes. **(b–e)** Before airflow exposure (magnification: 800×); **(b′–e′)** After 30 min of airflow exposure (magnification: 800×). Matching alphabetical labels indicate the same locations. Red circles highlight representative particle agglomerates that were observed to move or disappear after airflow exposure, indicating localized resuspension or rearrangement.

remains nearly constant, resulting in a relatively weaker adhesive force. In Fig. 11b′, a marked reduction in the number of particles on a specific fiber bundle is evident, suggesting the presence of localized high-velocity airflow. Considering that the perforated panel has an open-area ratio of about 4.5%, the local air velocity through each 6 mm hole can be estimated to be approximately 0.88 m/s under a total flow rate of 1000 m^3/h.

4. Discussion

4.1. Particle movement estimation after resuspension

The time series of indoor particle concentration measurements (Fig. 7) confirmed that, before the carpet installation, the background particle concentration was approximately 2.5×10^4 m^{-3} for particles in the 0.3–0.5 μm range, while the concentrations of larger particles were

significantly lower or nearly zero. When the carpet with deposited particles was installed, numerous peaks—interpreted as resuspension events—were observed. As the measurement height increased, both the amplitude and the frequency of these peaks decreased (Fig. 8). Although the particle number concentration was dominated by smaller particles (0.3–0.5 μm), the resuspension rate, when evaluated on a mass basis, increased with particle size under FSDV conditions (Figs. 10a–c). It should be noted, however, that the evaluation of resuspension rates under FSDV conditions was based on measurements obtained at 150 mm above the floor. Thus, the post-resuspension particle behavior requires further examination.

The behavior of particles after resuspension was analyzed by examining the balance between gravitational and aerodynamic drag forces—specifically, the relationship between the terminal settling velocity (v_g) and the area-averaged supply air velocity (v_u). The motion of a resuspended particle can be expressed by Newton's second law as the balance between gravitational and drag forces, as shown in Eq. (11):

$$m_p \frac{dv}{dt} = -F_D + F_g \tag{11}$$

where m_p is the mass of a single particle [kg], F_D is the aerodynamic drag force acting on a particle [N], and F_g is the gravitational force acting on a particle [N].

The aerodynamic drag force (F_D) acting on a particle moving in air is given by Eq. (12):

$$F_D = C_D A_p \cdot \rho_f \, v_r^2 / 2 \tag{12}$$

where C_D is the drag coefficient [–], A_p is the projected cross-sectional area of the particle ($= \pi D_p^2 / 4$) [m^2], ρ_f is the air density [kg/m^3], and v_r is the relative velocity between the particle and the surrounding airflow [m/s].

Since the particle Reynolds number (Re_p) calculated under all conditions was below 2, the drag coefficient was determined using Stokes' law, as shown in Eq. (13):

$$C_D = 24/Re_p \ : \ Re_p < 2 \tag{13}$$

where Re_p is the particle Reynolds number ($= \rho_f D_p v_r / \mu$) [–], D_p is the particle diameter [m], and μ is the dynamic viscosity of air [Pa·s].

By substituting Eq. (13) into Eq. (11) under steady-state conditions (dv/dt = 0), the terminal settling velocity v_g due to gravity can be expressed as Eq. (14):

$$v_g = (\rho_p - \rho_f) D_p^2 g \Big/ 18\mu \ : \ Re_p < 2 \tag{14}$$

where ρ_p is the particle density [kg/m^3] and g is the gravitational acceleration (9.81 m/s^2). The relationship between gravitational and drag forces acting on particles is illustrated in Fig. 12a.

The area-averaged supply air velocity v_u in the test chamber was calculated by dividing the exhaust airflow rate Q_e by the total chamber floor area A_c, as shown in Eq. (15):

$$v_u = Q_e / A_c \tag{15}$$

Finally, the estimated time (t_c) required for a particle to reach the ceiling height (H_c) can be derived from the relative velocity between the upward supply airflow (v_u) and the terminal settling velocity (v_g), as expressed in Eq. (16):

$$t_c = H_c / (v_u - v_g) \tag{16}$$

The results of this estimation are shown in Fig. 12b.

According to Fig. 12a, when comparing the balance between gravitational and aerodynamic drag forces, the upward supply airflow dominates for particles smaller than approximately 10 μm. Under the 1000 m^3/h and 750 m^3/h conditions, corresponding to ventilation rates of approximately 50 h^{-1} and 37 h^{-1}, respectively, which are considerably higher than those in typical office environments, the upward airflow exceeds the gravitational settling velocity even for particles larger than 10 μm. In contrast, under the 250 m^3/h condition (equivalent to 12.5 h^{-1}), gravitational settling becomes dominant for particles larger than about 10 μm. However, as shown in Fig. 8d, particles larger than 10 μm were rarely detected near the exhaust outlet. This is likely because the measurement point represented only a very small portion of the total exhaust area. The estimated time required for resuspended particles to reach the ceiling outlet was approximately 100 s under the 1000 m^3/h and 750 m^3/h conditions, and about 300 s under the 250 m^3/h condition (Fig. 12b). These findings suggest that, although the overall amount of resuspension is limited under typical ventilation rates (around 12–13 h^{-1}), once resuspended, particles may remain suspended in the room air for approximately five minutes before being exhausted.

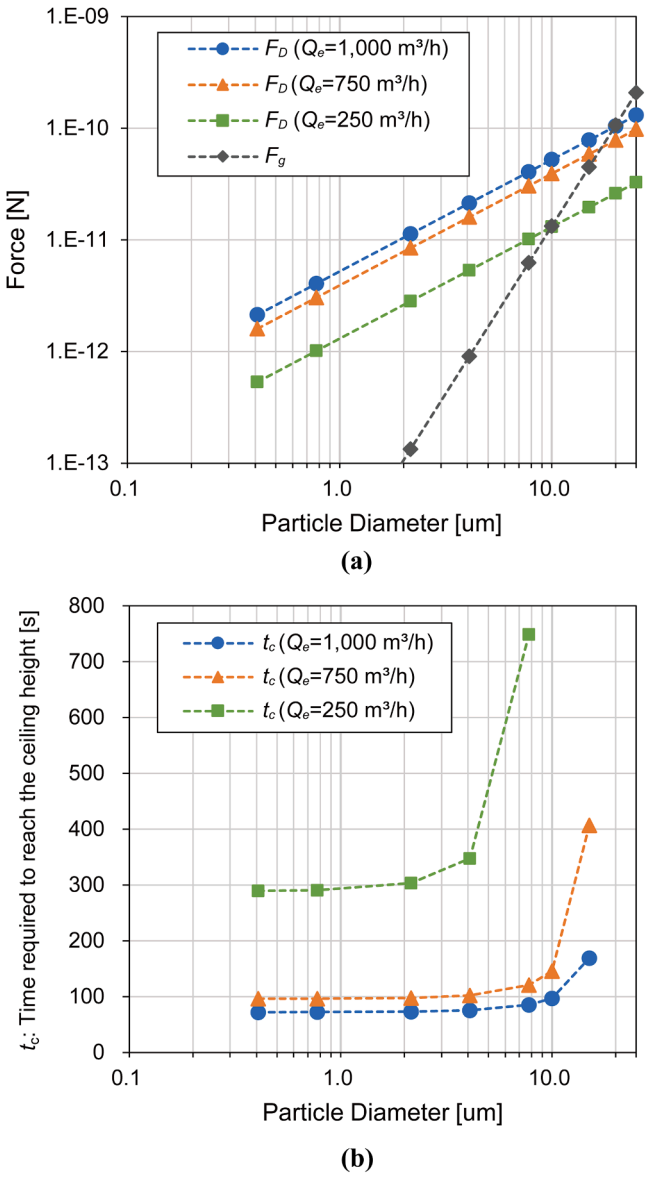

Fig. 12. Calculations for particle movement estimation. **(a)** Relationship between drag force (F_d) and gravitational force (F_g). **(b)** t_c: Time required to reach the ceiling height [s] under each ventilation volume.

4.2. Interpretation of key findings

Based on the obtained results, the key findings are summarized as follows.

Peaks attributed to resuspension were dominant in the smaller particle size range (0.3–0.5 μm) in terms of number concentration (Fig. 8). However, when evaluated in terms of mass, the resuspension rate tended to increase with particle size under FSDV conditions (Figs. 10a–c). From the balance between gravitational and aerodynamic forces, it was found that upward airflow dominated over gravity at 1000 m^3/h (50 ACH) and 750 m^3/h (37 ACH), whereas gravity became dominant for particles larger than approximately 10 μm at 250 m^3/h (13 ACH) (Fig. 12a). In Fig. 8a, few peaks were detected near the ceiling outlet under the 1000 m^3/h condition, likely because the resuspended particles became highly diluted before reaching the outlet and because the measurement point represented only a very small portion of the total exhaust area.

The effects of floor supply velocity (0.04, 0.03, and 0.01 m/s) and relative humidity (20%, 50%, and 80%) were pronounced. In particular, at 0.04 m/s, the resuspension rate increased significantly as relative humidity decreased, whereas at 0.01 m/s, the overall resuspension rates were small, and the influence of humidity was relatively minor (Figs. 10a–c). This behavior can be interpreted in terms of particle–surface adhesion mechanisms and aerodynamic forcing. Relative humidity is known to influence adhesion forces through multiple pathways. At higher humidity, capillary liquid bridges can form between particles and fibers, increasing adhesion forces and suppressing resuspension, particularly for aged carpets (Rosati et al., 2008) [46]. In the present study, the carpet was maintained in a near-pristine condition. In contrast, at lower humidity, electrostatic charging becomes more prominent, and repulsive electrostatic interactions between particles can reduce effective adhesion, leading to enhanced resuspension (Shaughnessy et al., 2012) [32]. In Fig. 10, the stronger humidity dependence observed at higher floor supply velocities suggests that, under sufficient aerodynamic forcing, variations in adhesion strength become a controlling factor for resuspension. At lower velocities (0.01 m/s), aerodynamic drag is insufficient to overcome adhesion forces regardless of humidity, resulting in uniformly low resuspension rates.

The particle-size dependence observed in the present study indicates that mass-based resuspension rates increase with particle diameter (Fig. 10). Close-up observations suggest that larger particles adhere to carpet fibers as agglomerates (Fig. 11). While the contact area between particle agglomerates and carpet fibers does not increase proportionally with particle size, the aerodynamic drag force increases with projected area. As a result, larger agglomerates experience a higher drag-to-adhesion force ratio, making them more susceptible to resuspension once detached.

The ventilation mode also had a substantial impact on resuspension behavior (Fig. 10). Under FSDV conditions, the resuspension rate ranged approximately from 10^{-8} to 10^{-4} h^{-1}, increasing with particle size. In contrast, under CCD conditions, the resuspension rate ranged from 10^{-5} to 10^{-3} h^{-1} for smaller particles (0.3–3 μm), but was nearly zero or even negative for larger particles ($\geq$ 10 μm). These results suggest that the dominant resuspension mechanisms differ between FSDV and CCD. Under FSDV conditions, microscopic observations (Fig. 11) indicated that particle agglomerates larger than 10 μm were more easily resuspended, as their exposed surface area to airflow was relatively large compared with their adhesion area, resulting in greater resuspension by the upward airflow. Conversely, under CCD conditions, resuspension likely occurred primarily for smaller particles that were less influenced by adhesive or gravitational forces, driven by the shear forces generated by horizontal airflow. After resuspension, these particles dispersed uniformly throughout the chamber. For particles larger than 10 μm, surface rolling or "saltation" motion may also have occurred. However, since the calculation methods used to estimate the resuspension rate differed between the two ventilation systems, the difference in magnitude alone cannot be used to conclude that CCD inherently produces greater resuspension than FSDV.

Microscopic observations further supported these findings. Noticeable changes were primarily observed in larger agglomerates exceeding 10 μm, and resuspension occurred locally in regions exposed to stronger airflow in FSDV. However, such changes were observed only in areas located directly above the 6 mm ventilation holes, whereas most other regions exhibited no noticeable change.

Regarding the order of airflow velocity, based on the opening ratio, the local air velocity through each 6 mm hole was estimated to be approximately 0.88 m/s under a total flow rate of 1000 m^3/h in the FSDV condition. However, in practice, a double-layer air-permeable carpet was installed above the perforated panel. As a result, the airflow reaching the carpet surface can be regarded as a seepage-type flow, and the effective near-surface velocity is considered to be on the order of the area-averaged supply velocity (0.01–0.04 m/s), rather than the locally estimated jet velocity. In the CCD condition with a total flow rate of 850 m^3/h, the airflow velocity was also measured using an ultrasonic anemometer (SONIC Corporation, DA-700; probe: TR-92T, 3 cm). At a height of 50 mm above the particle-distributed carpet, the 5-minute averaged horizontal velocity was approximately 0.50 m/s, and the absolute velocity magnitude was 0.55 m/s.

Based on these observations, although resuspension rates under CCD appear higher in magnitude for smaller particles (0.3–3 μm) than those under FSDV, this difference primarily reflects distinct airflow structures and calculation assumptions rather than inherently stronger resuspension. Near-floor velocity measurements indicate that CCD generates stronger horizontal shear close to the carpet surface, which preferentially mobilizes smaller particles. In contrast, FSDV produces low-velocity upward seepage flow, under which resuspension is governed by upward aerodynamic drag acting on particle agglomerates, leading to higher mass-based resuspension for coarse particles.

4.3. Comparison with previous studies

The resuspension rates obtained in this study ranged from approximately 10^{-8} to 10^{-4} h^{-1} under FSDV conditions and from 10^{-5} to 10^{-3} h^{-1} under CCD conditions. A wide range of resuspension rates has been reported in previous studies under various experimental conditions. In their review paper, Qian et al. (2014) [22] summarized numerous studies on resuspension caused by walking activities. For example, Gomes et al. (2007) [33] reported that the resuspension rate on quartz and roach-type carpets exposed to an airflow of 1.5 m/s ranged from 10^{-7} to 10^{-3} min^{-1} (equivalent to 10^{-6}–10^{-2} h^{-1}), which is comparable to the order of magnitude observed in this study. Qian et al. (2008) [37] estimated resuspension rates of 10^{-5}–10^{-2} h^{-1} during walking on carpeted floors, while Tian et al. (2014) [48] reported values in the range of 10^{-4}–10^{-1} h^{-1}.

Although the test particles and humidity conditions differed among studies, most investigations on walking-induced resuspension over carpeted floors under conventional ventilation systems reported rates within 10^{-4}–10^{-1} h^{-1} [22,23]. The values obtained in this study under FSDV conditions were lower than those reported for airflow shear–induced resuspension and substantially smaller than those induced by human walking, indicating that airflow-induced resuspension under FSDV conditions is relatively weak. At the very least, it can be concluded that FSDV does not promote particle resuspension more strongly than other ventilation methods. Furthermore, many previous studies have shown that larger particles tend to exhibit higher resuspension rates, which is consistent with the results obtained under FSDV conditions in this study [37,48,50].

The resuspension mechanisms are also known to differ significantly depending on the deposition structure. Specifically, particles deposited in multilayer configurations have been found to resuspend more readily than those forming a single layer [24,40]. As shown in the microscopic images (Fig. 11), most of the particles in this study formed multilayered aggregates adhering to the carpet fibers. These aggregated particle clusters —previously identified as "cluster feet" [24]— likely exhibited greater susceptibility to airflow drag forces due to their irregular shapes and exposed surface area, which may have facilitated their resuspension under FSDV conditions.

4.4. Limitations and implications for future work

- This study has several limitations that should be acknowledged:
- The mass fraction of test particles in each size class (f_p) was referenced from Y. Takeuchi et al. (2022) [47]. However, the actual particle size distribution on the carpet may have been biased toward larger diameters, as suggested by Fig. 11. Higher-magnification microscopic analysis would enable a more accurate estimation of f_p.
- Under FSDV conditions, resuspension rates were calculated using particle concentrations measured at 150 mm above the carpet surface. This height was selected as a conservative evaluation point, where the influence of gravitational settling of coarse particles and horizontal turbulent dispersion is minimized, and the assumption underlying the conversion factor α remains valid. Although particle size distributions may vary with height due to settling effects, the characterization of such vertical dependence is identified as a topic for future investigation.
- Ryukakusan was used as a surrogate test particle and was validated against Arizona Test Dust A1 through additional comparative experiments (Appendix C), showing resuspension rates of the same order of magnitude. Although neither material directly represents infectious droplets, Ryukakusan provides a practical and reproducible surrogate for airflow-induced resuspension under the present conditions.
- Because ambient humidity during particle dispersion in the entrance hall also affects adhesive forces, improved humidity control during the dispersion process would allow for more accurate comparisons among test conditions.
- Since humidity control in this study was achieved through temperature adjustments, the temperature varied from 17°C to 36°C across the experimental cases (Table B-1). Maintaining a uniform temperature across all test conditions could further enhance the reliability of comparative analysis.
- Under conditions with a floor supply velocity of 0.010 m/s, the overall resuspension was extremely low. Consequently, adhesive forces and temperature variations may have exerted relatively strong influences, potentially reducing the reproducibility of the results.
- As shown in Appendix C, the calculated resuspension rate can become zero when no distinct resuspension peaks are detected during the observation period, even under nominally identical conditions. This intermittency-related uncertainty is more pronounced in coarse particle size ranges, where resuspension events occur less frequently. Although repeated CCD experiments would be required for more robust uncertainty quantification, this limitation does not affect the main qualitative conclusion that CCD tends to yield higher resuspension rates than FSDV in smaller particle size ranges.
- Ideally, all experimental conditions should be repeated to improve statistical robustness. In the present study, full repetition was not feasible due to resource constraints; however, repeated experiments were conducted under a representative FSDV condition (FSDV_0.04_50), and the resulting variability is reported in Appendix C. The observed intermittency and sensitivity to peak detection, particularly for coarse particles, do not alter the main qualitative conclusions of this study.

In future studies, it will be important to clarify the quantitative relationship between particle resuspension and infection risk. Additionally, experimental investigations should be conducted to evaluate resuspension rates under FSDV airflow when external disturbances such as walking or falling objects are present.

5. Conclusion

This study experimentally evaluated the resuspension behavior of fine particles deposited on an air-permeable carpet under floor supply displacement ventilation (FSDV) airflow, with circular ceiling diffuser (CCD; Anemostat-type diffuser) conditions included for comparison. By systematically varying floor supply velocity and relative humidity, the study provides one of the first experimental datasets characterizing resuspension behavior specific to FSDV airflow.

The results demonstrate that airflow-induced resuspension under FSDV remains limited in magnitude and is substantially smaller than walking-induced resuspension reported in previous studies [22,23], even at relatively high air exchange rates. In particular, under the 12 ACH condition, which corresponds to the carpet's recommended operating range, resuspension was consistently low, indicating that FSDV does not inherently increase the risk of particle resuspension when properly designed and operated. The findings further highlight that resuspension behavior under FSDV differs fundamentally from that under CCD, reflecting differences in airflow structure, dominant forces acting on particles, and applicable calculation assumptions.

From a practical perspective, this study introduces and validates an experimental framework for quantifying particle resuspension under non-uniform, low-velocity ventilation systems such as FSDV, where conventional room-averaged approaches are not directly applicable. The additional comparative experiments with Arizona Test Dust further support the robustness of the adopted methodology.

Future research should extend the present approach to scenarios involving mechanical disturbances, such as human walking, and explore spatial variability using repeated measurements or complementary modeling techniques. The results of this study are expected to support HVAC designers and engineers in making evidence-based decisions when selecting ventilation strategies for medical and cleanroom environments, particularly in balancing infection control performance and particle resuspension risk.

Declaration of generative AI and AI-assisted technologies in the writing process

During the preparation of this work, the author used ChatGPT (OpenAI) in order to improve the clarity, language, and style of the manuscript. After using this tool, the author reviewed and edited the content as needed and takes full responsibility for the content of the published article.

Data availability

Data will be made available on request.

CRediT authorship contribution statement

Jun Yoshihara: Writing – review & editing, Writing – original draft, Validation, Resources, Methodology, Investigation, Formal analysis, Data curation, Conceptualization. **Toshio Yamanaka:** Writing – review & editing, Validation, Supervision, Project administration, Funding acquisition, Conceptualization. **Tomohiro Kobayashi:** Validation, Supervision, Project administration, Funding acquisition, Conceptualization. **Haruna Yamasawa:** Supervision. **Noriaki Kobayashi:** Methodology, Conceptualization. **Hisako Nagata:** Resources, Project administration, Conceptualization. **Shigeru Okamoto:** Writing – review & editing, Conceptualization.

Declaration of competing interest

The authors declare that they have no known competing financial interests or personal relationships that could have appeared to influence the work reported in this paper.

Acknowledgements

This work was supported by JST SPRING, Grant Number JPMJSP2138, and JSPS KAKENHI Grant Number 25KJ1753 (Principal

Investigator, Jun Yoshihara). The authors would like to express their sincere gratitude to Mrs. Saori Yasui and Mr. Kazuki Sugita of Tohata Architects & Engineers, Inc. for their valuable comments and discussions during the research. The authors also extend their deep appreciation to Professor Yoshiko Takeuchi of Gifu Pharmaceutical University for her valuable advice and cooperation regarding the test particles.

Appendix A. Validation of uniform particle distribution

An experiment was conducted to verify the uniformity of particle distribution from the powder-spraying device shown in Fig. 4. The test conditions were identical to those used in the main experiment, including the spraying height and device. Twenty-five Petri dishes (100 × 100 mm each) were arranged in a 5 × 5 grid on the deposition surface, and the increase in mass of each dish was measured using a tuning fork-type electronic balance (RJ-620, Shinko Denshi Co., Ltd.; minimum resolution: 0.001 g). The upper opening of the wind shield was divided into sixteen equal sections (Fig. 5a). From each section, fifteen sprays were applied sequentially in rotation, rather than repeatedly at the same point, to prevent localized accumulation. Each spraying cycle required approximately ten minutes to complete, and the entire procedure was repeated three times.

Photographs taken after spraying, the measured mass increases, and their relative spatial distributions are presented in Fig. A-1, while the total and statistical results (mean and standard deviation) are summarized in Table A-1. As seen in Fig. A-1 (a, d, g), the visual appearance differed noticeably between the first and the second/third trials. This variation is attributed to differences in ambient relative humidity between test days, which likely altered the surface condition of the Petri dishes. In the ideal case, each of the twenty-five dishes would account for 4% of the total mass increase. The experimental results (Fig. A-1 c, f, i) showed that all dishes fell within 4 ± 0.5 %. According to Table A-1, the total mass increase across all dishes was 0.971 ± 0.097 g, corresponding to an average increase of 0.339 ± 0.004 g per dish. The ratio of the standard deviation to the mean for individual dishes was 0.091, confirming that the particle distribution achieved uniformity within approximately 1 %.

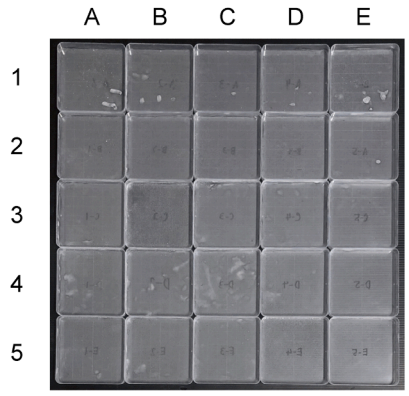

(a)

	A	B	C	D	E
1	0.034 g	0.032 g	0.031 g	0.034 g	0.031 g
2	0.033 g	0.035 g	0.036 g	0.035 g	0.030 g
3	0.032 g	0.034 g	0.037 g	0.039 g	0.033 g
4	0.037 g	0.038 g	0.040 g	0.038 g	0.033 g
5	0.035 g	0.038 g	0.036 g	0.034 g	0.033 g

(b)

	A	B	C	D	E
1	3.9 %	3.7 %	3.6 %	3.9 %	3.6 %
2	3.8 %	4.0 %	4.1 %	4.0 %	3.5 %
3	3.7 %	3.9 %	4.3 %	4.5 %	3.8 %
4	4.3 %	4.4 %	4.6 %	4.4 %	3.8 %
5	4.0 %	4.4 %	4.1 %	3.9 %	3.8 %

(c)

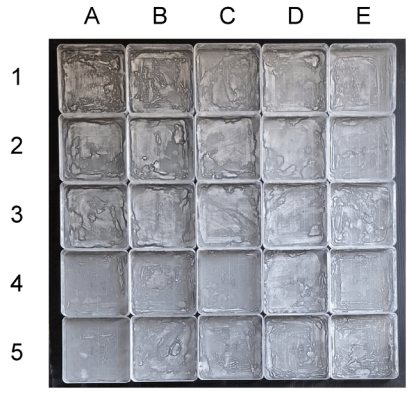

(d)

	A	B	C	D	E
1	0.043 g	0.041 g	0.041 g	0.049 g	0.044 g
2	0.034 g	0.043 g	0.045 g	0.048 g	0.044 g
3	0.039 g	0.047 g	0.048 g	0.051 g	0.042 g
4	0.038 g	0.042 g	0.042 g	0.047 g	0.040 g
5	0.034 g	0.039 g	0.040 g	0.041 g	0.039 g

(e)

	A	B	C	D	E
1	4.1 %	3.9 %	3.9 %	4.6 %	4.1 %
2	3.2 %	4.1 %	4.2 %	4.5 %	4.1 %
3	3.7 %	4.4 %	4.5 %	4.8 %	4.0 %
4	3.6 %	4.0 %	4.0 %	4.4 %	3.8 %
5	3.2 %	3.7 %	3.8 %	3.9 %	3.7 %

(f)

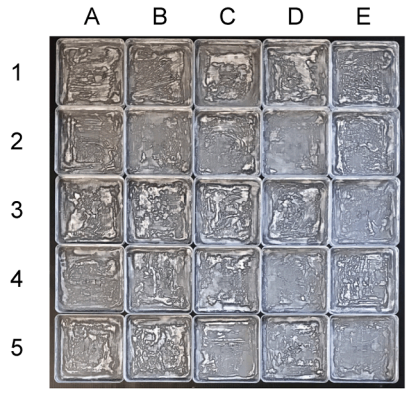

(g)

	A	B	C	D	E
1	0.037 g	0.036 g	0.041 g	0.044 g	0.038 g
2	0.034 g	0.036 g	0.039 g	0.040 g	0.039 g
3	0.035 g	0.043 g	0.044 g	0.044 g	0.037 g
4	0.033 g	0.039 g	0.040 g	0.037 g	0.038 g
5	0.039 g	0.044 g	0.045 g	0.046 g	0.035 g

(h)

	A	B	C	D	E
1	3.8 %	3.7 %	4.2 %	4.5 %	3.9 %
2	3.5 %	3.7 %	4.0 %	4.1 %	4.0 %
3	3.6 %	4.4 %	4.5 %	4.5 %	3.8 %
4	3.4 %	4.0 %	4.1 %	3.8 %	3.9 %
5	4.0 %	4.5 %	4.6 %	4.7 %	3.6 %

(i)

Fig. A-1. Results of spraying powder onto Petri dishes from a height of 400 mm using the device shown in Fig. 4(b) (240 sprays). **(a, d, g)** Photographs after spraying; **(b, e, h)** Increase in dish weight [g]; **(c, f, i)** Relative contribution of each dish to the total weight increase [%]. **(a–c)** First trial; **(d–f)** Second trial; **(g–i)** Third trial.

Table A-1
Deposited powder mass on Petri dishes in three spraying trials (240 sprays per trial).

Trial	Total [g]	Average [g]	SD [g]	CV [-]
1	0.868	0.035	0.003	0.077
2	1.061	0.042	0.004	0.102
3	0.983	0.039	0.004	0.094
Mean ± SD	0.971 ± 0.097	0.039 ± 0.004	0.004	0.091

The average mass increase per Petri dish was calculated as the total divided by 25. SD: Standard deviation of the mass increase among the 25 Petri dishes; CV: Coefficient of variation (SD / Average). The bottom row presents the mean ± SD across the three trials. For SD and CV, only the mean

values are shown.

Appendix B. Temperature and relative humidity during the experiments

Details of the temperature, relative humidity, ventilation rate, and mass of the dispersed powder during the experiments are summarized in Table B-1.

Table B-1
Details of experimental conditions measured in each test.

Test name	*RH*(*t*) [%]	*T*(*t*) [°C]	*AH*(*t*) [g/m^3]	*RH*(*s*) [%]	*T*(*s*) [°C]	*AH*(*s*) [g/m^3]	*RH*(*e*) [%]	*T*(*e*) [°C]	*AH*(*e*) [g/m^3]	Q_e [m^3/h]	L_{Total} [g]
FSDV_0.04_20	19.2 ± 0.4	28.1 ± 0.1	5.23 ± 0.11	36.2 ± 0.3	20.3 ± 0.1	6.37 ± 0.03	38.2 ± 0.4	19.3 ± 0.1	6.34 ± 0.06	990	1.001
FSDV_0.04_50	53.2 ± 5.3	18.7 ± 0.6	8.54 ± 0.97	52.9 ± 0.8	19.9 ± 0.0	9.08 ± 0.14	54.1 ± 0.1	19.9 ± 0.1	9.30 ± 0.06	990	1.014
FSDV_0.04_80	82.3 ± 0.8	17.3 ± 0.2	12.11 ± 0.05	69.0 ± 0.9	18.7 ± 0.0	11.08 ± 0.14	66.8 ± 0.4	18.3 ± 0.1	10.46 ± 0.04	990	0.992
FSDV_0.03_20	19.3 ± 0.5	33.3 ± 0.1	6.97 ± 0.20	35.9 ± 0.3	25.4 ± 0.1	8.45 ± 0.07	40.3 ± 0.6	23.2 ± 0.1	8.40 ± 0.13	748 ± 4	1.019
FSDV_0.03_50	49.8 ± 1.1	21.6 ± 0.3	9.47 ± 0.16	60.4 ± 0.4	19.7 ± 0.0	10.25 ± 0.04	60.3 ± 0.4	19.7 ± 0.1	10.27 ± 0.06	757 ± 9	1.002
FSDV_0.03_80	79.2 ± 0.5	17.7 ± 0.1	11.93 ± 0.09	69.8 ± 0.3	18.8 ± 0.0	11.24 ± 0.05	70.3 ± 0.3	18.2 ± 0.1	10.94 ± 0.09	740 ± 7	1.009
FSDV_0.01_20	16.7 ± 0.5	28.0 ± 0.4	4.55 ± 0.14	39.8 ± 1.5	18.7 ± 0.1	6.37 ± 0.22	42.7 ± 0.7	17.1 ± 0.2	6.23 ± 0.17	241 ± 1	1.001
FSDV_0.01_50	43.0 ± 6.3	19.1 ± 0.7	7.04 ± 0.82	45.2 ± 1.8	22.1 ± 0.1	8.84 ± 0.37	44.8 ± 0.8	22.2 ± 0.4	8.77 ± 0.24	246 ± 1	0.999
FSDV_0.01_80	73.3 ± 3.9	21.6 ± 0.1	13.90 ± 0.69	73.4 ± 0.8	22.1 ± 0.0	14.35 ± 0.15	73.5 ± 0.5	22.0 ± 0.3	14.17 ± 1.31	246 ± 1	0.986
CCD_850_50	46.4 ± 0.7	36.5 ± 0.1	19.88 ± 0.25	58.8 ± 0.5	33.0 ± 0.1	20.98 ± 0.14	57.0 ± 0.8	33.1 ± 0.1	20.44 ± 0.17	848 ± 10	1.024
CCD_750_50	45.4 ± 1.6	27.9 ± 0.2	12.28 ± 0.35	62.4 ± 0.6	24.7 ± 0.1	14.13 ± 0.11	64.6 ± 0.4	24.3 ± 0.0	14.31 ± 0.07	756 ± 6	1.003
CCD_250_50	46.3 ± 0.8	23.9 ± 0.2	10.00 ± 0.16	48.8 ± 0.8	25.1 ± 0.2	11.32 ± 0.12	48.2 ± 0.5	25.7 ± 0.1	11.58 ± 0.09	254 ± 1	1.024
FSDV_0.04_20_no	21.0 ± 0.6	27.0 ± 0.4	5.42 ± 0.11	35.9 ± 1.6	20.1 ± 0.6	6.24 ± 0.07	36.7 ± 1.1	18.8 ± 0.1	5.90 ± 0.21	990	-
CCD_850_50_no	49.1 ± 1.1	35.4 ± 0.2	19.88 ± 0.29	60.7 ± 0.6	32.3 ± 0.2	20.80 ± 0.05	60.0 ± 0.3	32.3 ± 0.1	20.64 ± 0.02	848 ± 10	-

Measurement locations are shown in Fig. 2. (*t*): Test chamber; (*s*): Surrounding space; (*e*): Entrance hall. Values are expressed as mean ± standard deviation over the experimental duration, except for L_{total} . *AH* is calculated from *RH* and *T* using Eqs. 1-3. Q_e is calculated from the CO_2 balance measured in exhaust duct. $Q_e = 990$ m^3/h indicates the set value of the constant air volume system (CAV); the ventilation volume was automatically adjusted.

Appendix C. Repeated Experiments Comparing Ryukakusan and Arizona Test Dust under FSDV Conditions

To examine the suitability of Ryukakusan as a test particle, repeated experiments were conducted using both Ryukakusan (RKS) and Arizona Test Dust A1 (ATD) under identical FSDV conditions. The experiments were performed at a total airflow rate of 1000 m^3/h ($v_f = 0.040$ m/s, 50 ACH) with a target relative humidity of 50%, which represents a typical operating condition in office and medical environments. These repeated tests also served to quantify experimental variability under the same conditions as FSDV_0.04_50 in the main text.

Five repeated experiments were conducted for each test particle (RKS and ATD). Table C-1 summarizes the experimental conditions and the measured environmental variables, including relative humidity, temperature, absolute humidity, exhaust airflow rate, and applied particle mass. Although slight variations in temperature and humidity were observed among test cases, the tests were conducted within a comparable indoor environmental range.

Table C-1
Experimental conditions and measured environmental values for repeated tests.

Test name	RH(*t*) [%]	T(*t*) [℃]	AH(*t*) [g/m^3]	Q_e [m^3/h]	L_{Total} [g]
RKS_1	53.2 ± 5.3	18.7 ± 0.6	8.54 ± 0.97	990	1.014
RKS_2	50.8 ± 0.3	22.9 ± 0.1	10.37 ± 0.03	990	1.037
RKS_3	49.8 ± 0.1	23.1 ± 0.0	10.27 ± 0.03	990	1.044
RKS_4	49.6 ± 0.3	23.1 ± 0.1	10.27 ± 0.03	990	1.041
RKS_5	49.0 ± 0.1	23.2 ± 0.0	10.21 ± 0.03	990	1.026
ATD_1	50.2 ± 0.2	21.7 ± 0.0	9.57 ± 0.05	990	1.022
ATD_2	50.7 ± 0.2	21.8 ± 0.0	9.71 ± 0.04	990	1.018
ATD_3	51.2 ± 0.3	21.8 ± 0.0	9.81 ± 0.06	990	1.043
ATD_4	49.9 ± 0.3	21.8 ± 0.0	9.57 ± 0.07	990	1.050
ATD_5	52.6 ± 0.7	8.3 ± 0.2	4.44 ± 0.02	990	1.030

Fig. C-1a and C-1b show the size-resolved resuspension rates obtained from the five repeated tests for RKS and ATD, respectively, while Fig. C-1c

compares the mean values with ±1 standard deviation (n = 5).

For both particles, the resuspension rate generally increased with particle diameter, particularly for particles larger than 5 μm. Despite some scatter among individual trials, especially in the larger size ranges, the overall trends were broadly consistent between RKS and ATD. Notably, for ATD, several size ranges above 3 μm yielded zero or negative values. This is likely because, for larger particles, the calculated resuspension rate becomes highly sensitive to whether discrete resuspension peaks are detected; if a peak occurs, the rate increases markedly because the mass per particle is large. Overall, these results indicate that the present experiments quantify resuspension within a very low range, where run-to-run variability can be non-negligible. Based on these repeated tests, the measurement uncertainty (±1 SD) obtained for RKS under FSDV_0.04_50 was represented in Fig. 10a in the main text for the corresponding condition.

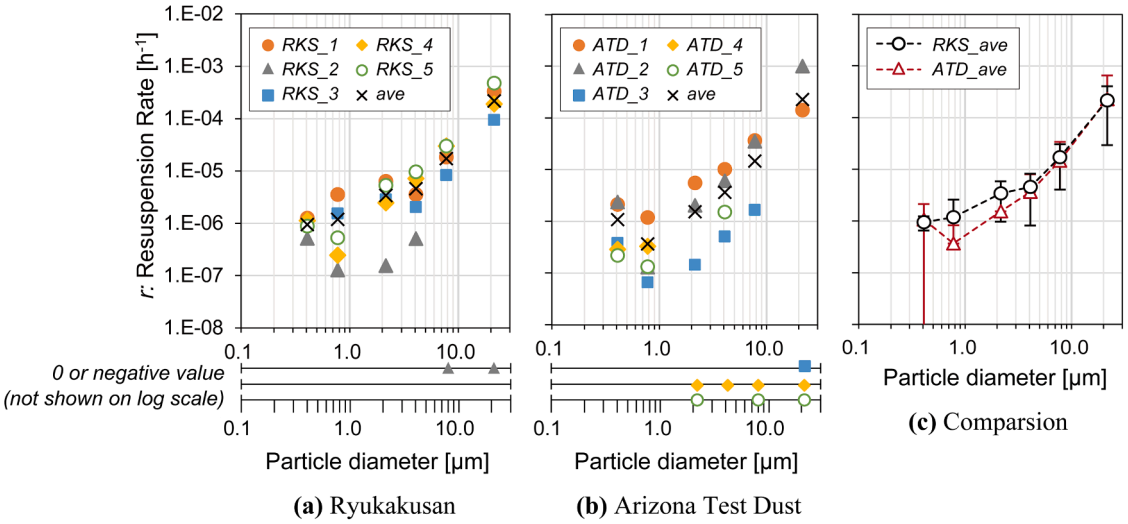

Fig. C-1. Size-resolved resuspension rates obtained from repeated tests under FSDV_0.04_50. **(a)** Ryukakusan (RKS). **(b)** Arizona Test Dust A1 (ATD). **(c)** Comparison of mean values with ±1 standard deviation (n = 5). For ATD, the mean minus one standard deviation becomes negative in some size ranges ≥ 0.5 μm due to intermittency and near-zero resuspension in several repeated tests, and are therefore not shown below zero on the logarithmic scale.

To quantitatively assess the agreement between the two test particles, the ratio of the mean resuspension rates for ATD and RKS (ATD_ave/RKS_ave) was calculated for each particle size range. The ratios were 1.14 (0.3–0.5 μm), 0.31 (0.5–1.0 μm), 0.45 (1.0–3.0 μm), 0.80 (3.0–5.0 μm), 0.85 (5.0–10.0 μm), and 1.04 (≥10 μm). These results show that, although differences were observed in the submicron range, the resuspension rates of RKS and ATD remained within the same order of magnitude across all size ranges. In particular, for particles larger than 3 μm—which contribute more substantially to mass-based resuspension—the ratios were close to unity (0.80–1.04).

Overall, these repeated-test results indicate that Ryukakusan exhibits resuspension behavior comparable to ATD under the present FSDV airflow condition, especially in the larger particle size ranges relevant to mass-based resuspension. Therefore, Ryukakusan is considered a reasonable surrogate test particle for evaluating airflow-induced resuspension from carpets under the present experimental conditions, with practical advantages in terms of handling safety.

Data availability

Data will be made available on request.

References

[1] R.W. Hyland, A. Wexler, Formulations for the thermodynamic properties of dryair from 173.15 K to 373.15 K, at pressures to 5 MPa, ASHRAe Trans. (1989).
[2] World Health Organization, WHO COVID-19 dashboard, (n.d.). https://data.who.int/dashboards/covid19/cases?n=c (accessed September 10, 2025).
[3] World Health Organization, Coronavirus disease (COVID-19): how is it transmitted?, (2021). https://www.who.int/emergencies/diseases/novel-coronavirus-2019/question-and-answers-hub/q-a-detail/coronavirus-disease-covid-19-how-is-it-transmitted (accessed September 10, 2025).
[4] Healthcare Engineering Association of Japan (HEAJ), Hospital Facilities Design Guidelines (Air conditioning volume), HEAS-02-2022, 2022.
[5] U.S. Department of Health, H. Services, C. for Disease Control, Guidelines for Environmental Infection Control in Health-Care Facilities Recommendations of CDC and the Healthcare Infection Control Practices Advisory Committee (HICPAC), 2019.
[6] Japanese Ministry of Health Labour and Welfare, How to prevent Wide Spread Outbreak | COVID-19 Information and Resouces. COVID-19 May Spread through the Following Routes, 2022. https://corona.go.jp/en/prevention/. accessed November 17, 2022.
[7] Y. Li, H. Qian, J. Hang, X. Chen, P. Cheng, H. Ling, S. Wang, P. Liang, J. Li, S. Xiao, J. Wei, L. Liu, B.J. Cowling, M. Kang, Probable airborne transmission of SARS-CoV-2 in a poorly ventilated restaurant, Build. Environ. 196 (2021) 107788, https://doi.org/10.1016/J.BUILDENV.2021.107788.
[8] Federation of European Heating Ventilation and Air Conditioning Associations, COVID-19 guidance document version 4.0; how to operate HVAC and other building service systems to prevent the spread of the coronavirus (SARS-CoV-2) disease (COVID-19) in workplaces, 2020.
[9] W. Su, B. Yang, A. Melikov, C. Liang, Y. Lu, F. Wang, A. Li, Z. Lin, X. Li, G. Cao, R. Kosonen, Infection probability under different air distribution patterns, Build. Environ. 207 (2022), https://doi.org/10.1016/j.buildenv.2021.108555.
[10] A. Melikov, A. Li, R. Kosonen, X. Li, Occupant targeted ventilation brings clean air to occupants, REHVA Eur. HVAC J. (2022). https://www.researchgate.net/publication/358915595.
[11] J. Yoshihara, T. Yamanaka, N. Choi, T. Kobayashi, H. Yamasawa, N. Kobayashi, H. Nagata, S. Okamoto, S. Yasui, K. Sugita, A. Fujiwara, Performance of local exhaust system as prevention measure of infection in consulting room, Part 11 Eff. Air Flow Rate Infect. Risk Var. Under floor Air Supply Syst. Jpn. (2024).
[12] P.V Nielsen, Displacement Ventilation - theory and design, Aalborg University, 1993. https://vbn.aau.dk/ws/portalfiles/portal/36323578/Displacement+Ventilation+-+theory+and+design+%28gul+serie%29.pdf. accessed May 24, 2024.
[13] X. Yuan, Q. Chen, L.R. Glicksman, A critical review of displacement ventilation, AIVC 4101 (1998) 1–13. https://www.aivc.org/resource/critical-review-displacement-ventilation. accessed November 26, 2022.
[14] N. Gao, J. Niu, L. Morawska, Distribution of respiratory droplets in enclosed environments under different air distribution methods, Build. Simul. 4 (1) (2008) 326–335, https://doi.org/10.1007/S12273-008-8328-0, 2008 1.
[15] J. Wei, Y. Li, Airborne spread of infectious agents in the indoor environment, Am. J. Infect. Control 44 (2016) S102–S108, https://doi.org/10.1016/J.AJIC.2016.06.003.
[16] R.K. Bhagat, P.F. Linden, Displacement ventilation: A viable ventilation strategy for makeshift hospitals and public buildings to contain COVID-19 and other airborne diseases: ventilation strategy for COVID-19, R. Soc. Open. Sci. 7 (2020), https://doi.org/10.1098/RSOS.200680.
[17] J. Yoshihara, T. Yamanaka, N. Choi, T. Kobayashi, N. Kobayashi, A. Fujiwara, Infection-prevention performance of local exhaust ventilation under three different underfloor air distribution systems during a face-to-face conversation, Build. Environ. 265 (2024), https://doi.org/10.1016/j.buildenv.2024.111911.

[18] K. Zhang, X. Zhang, S. Li, X. Jin, Review of underfloor air distribution technology, Energy Build. 85 (2014) 180–186, https://doi.org/10.1016/J.ENBUILD.2014.09.011.
[19] K.J. Loudermilk, Underfloor air distribution solutions for open office applications, ASHRAe Trans. (1999) 605–613. https://www.aivc.org/resource/underfloor-air-distribution-solutions-open-office-applications. accessed November 28, 2022.
[20] J. Yoshihara, T. Yamanaka, T. Kobayashi, N. Choi, N. Kobayashi, Performance of combination of local exhaust system and floor-supply displacement ventilation system as prevention measure of infection in consulting room, Jpn. Arch. Rev. 6 (2023), https://doi.org/10.1002/2475-8876.12413.
[21] G.A. Sehmel, Particle resuspension: A review, Environ. Int. 4 (1980) 107–127.
[22] J. Qian, J. Peccia, A.R. Ferro, Walking-induced particle resuspension in indoor environments, Atmos. Environ. 89 (2014) 464–481, https://doi.org/10.1016/j.atmosenv.2014.02.035.
[23] F. Yuan, R. Yao, W. Yu, S. Sadrizadeh, H. Awbi, P. Kumar, Dynamic characteristics of particulate matter resuspension due to human activities in indoor environments: a comprehensive review, J. Build. Eng. 79 (2023), https://doi.org/10.1016/j.jobe.2023.107914.
[24] C. Henry, J.P. Minier, Progress in particle resuspension from rough surfaces by turbulent flows, Prog. Energy Combust. Sci. 45 (2014) 1–53, https://doi.org/10.1016/j.pecs.2014.06.001.
[25] Y. Kubota, H. Higuchi, Aerodynamic particle resuspension due to human foot and model foot motions, Aerosol Sci. Technol. 47 (2013) 208–217, https://doi.org/10.1080/02786826.2012.742486.
[26] T.L. Thatcher, D.W. Layton, Deposition, resuspension, and penetration of particles within a residence, 1995.
[27] M. Luoma, S.A. Batterman, Characterization of particulate emissions from occupant activities in offices, Indoor. Air. 11 (2001) 35–48, https://doi.org/10.1034/j.1600-0668.2001.011001035.x.
[28] J. Qian, A.R. Ferro, K.R. Fowler, Estimating the resuspension rate and residence time of indoor particles, J. Air Waste Manag. Assoc. 58 (2008) 502–516, https://doi.org/10.3155/1047-3289.58.4.502.
[29] E. Abt, H.H. Suh, P. Catalano, P. Koutrakis, Relative contribution of outdoor and indoor particle sources to indoor concentrations, Environ. Sci. Technol. 34 (2000) 3579–3587, https://doi.org/10.1021/es990348y.
[30] J. Ren, M. Wade, R.L. Corsi, A. Novoselac, Particulate matter in mechanically ventilated high school classrooms, Build. Environ. 184 (2020), https://doi.org/10.1016/j.buildenv.2020.106986.
[31] G. Pei, J.D. Freihaut, D. Rim, Long-term application of low-cost sensors for monitoring indoor air quality and particle dynamics in a commercial building, J. Build. Eng. 79 (2023), https://doi.org/10.1016/j.jobe.2023.107774.
[32] R. Shaughnessy, H. Vu, Particle loadings and resuspension related to floor coverings in chamber and in occupied school environments, Atmos. Environ. 55 (2012) 515–524, https://doi.org/10.1016/j.atmosenv.2012.04.008.
[33] C. Gomes, J. Freihaut, W. Bahnfleth, Resuspension of allergen-containing particles under mechanical and aerodynamic disturbances from human walking, Atmos. Environ. 41 (2007) 5257–5270, https://doi.org/10.1016/j.atmosenv.2006.07.061.
[34] M.P. Buttner, P. Cruz-Perez, L.D. Stetzenbach, P.J. Garrett, A.E. Luedtke, Measurement of airborne fungal spore dispersal from three types of flooring materials, 2002.
[35] H. Zhang, H. Liu, A.R. Ferro, A.C.K.L Vivian, Effects of triboelectric charging, flooring materials, relative humidity, and shoe sole materials on human walking-induced particle resuspension, Build. Environ. 244 (2023), https://doi.org/10.1016/j.buildenv.2023.110838.
[36] S.Y. Yang, H.H. Zhang, T.C. Hsiao, A.R. Ferro, A.C.K. Lai, Evaluation of human walking-induced resuspension of bacteria on different flooring materials, Build. Environ. 235 (2023), https://doi.org/10.1016/j.buildenv.2023.110218.
[37] J. Qian, A.R. Ferro, Resuspension of dust particles in a chamber and associated environmental factors, Aerosol Sci. Technol. 42 (2008) 566–578, https://doi.org/10.1080/02786820802220274.
[38] H.K. Hyytiäinen, B. Jayaprakash, P.V. Kirjavainen, S.E. Saari, R. Holopainen, J. Keskinen, K. Hämeri, A. Hyvärinen, B.E. Boor, M. Täubel, Crawling-induced floor dust resuspension affects the microbiota of the infant breathing zone, Microbiome 6 (2018), https://doi.org/10.1186/s40168-018-0405-8.
[39] T. Wu, M. Täubel, R. Holopainen, A.K. Viitanen, S. Vainiotalo, T. Tuomi, J. Keskinen, A. Hyvärinen, K. Hämeri, S.E. Saari, B.E. Boor, Infant and adult inhalation exposure to resuspended biological particulate matter, Environ. Sci. Technol. 52 (2018) 237–247, https://doi.org/10.1021/acs.est.7b04183.
[40] B.E. Boor, J.A. Siegel, A. Novoselac, Monolayer and multilayer particle deposits on hard surfaces: literature review and implications for particle resuspension in the indoor environment, Aerosol Sci. Technol. 47 (2013) 831–847, https://doi.org/10.1080/02786826.2013.794928.
[41] C. Henry, J.P. Minier, S. Brambilla, Particle resuspension: challenges and perspectives for future models, Phys. Rep. 1007 (2023) 1–98, https://doi.org/10.1016/j.physrep.2022.12.005.
[42] K. Hayato, T. Yasunobu, K. Yu, K. Toshiki, Y. Toshio, N. Hisako, O. Shigeru, Y. Saori, Verification of particles behavior due to differences in air conditioning methods (in Japanese), Trans. Soc. Heat. Air-Cond. Sanit. Eng. Jpn. 47 (2022) 1–11.
[43] Y. Kim, G. Wellum, K. Mello, K.E. Strawhecker, R. Thoms, A. Giaya, B.E. Wyslouzil, Effects of relative humidity and particle and surface properties on particle resuspension rates, Aerosol Sci. Technol. 50 (2016) 339–352, https://doi.org/10.1080/02786826.2016.1152350.
[44] P. Salimifard, D. Rim, C. Gomes, P. Kremer, J.D. Freihaut, Resuspension of biological particles from indoor surfaces: effects of humidity and air swirl, Sci. Total Environ. 583 (2017) 241–247, https://doi.org/10.1016/j.scitotenv.2017.01.058.
[45] ISO, INTERNATIONAL STANDARD, ISO 7726, Ergonomics of the thermal environment-Instruments for measuring physical quantities, 2nd ed., 1998. https://standards.iteh.ai/catalog/standards/sist/99f92eea-d1b3-48b4-8a3c-.
[46] J.A. Rosati, J. Thornburg, C. Rodes, Resuspension of particulate matter from carpet due to human activity, Aerosol Sci. Technol. 42 (2008) 472–482, https://doi.org/10.1080/02786820802187069.
[47] Y. Takeuchi, T. Nakatsubo, A. Fukui, R. Fujii, K. Tahara, H. Takeuchi, Design of a medicine spoon for an herbal powder and evaluation of the powders flowability–In a case of an herbal powder formulated as an antitussive and expectorant–(in Japanese), J. Pharm. Sci. Technol., Jpn. 77 (2017) 164–176.
[48] Y. Tian, K. Sul, J. Qian, S. Mondal, A.R. Ferro, A comparative study of walking-induced dust resuspension using a consistent test mechanism, Indoor. Air. 24 (2014) 592–603, https://doi.org/10.1111/ina.12107.
[49] ANSI/ASHRAE/ASHE, ANSI/ASHRAE/ASHE Standard 170-2017, ventilation of Health Care Facilities, 2020. https://www.ashrae.org/technical-resources/standards-and-guidelines/standards-addenda/ansi-ashrae-ashe-standard-170-2017-ventilation-of-health-care-facilities (accessed January 29, 2026).
[50] A. Benabed, A. Boulbair, PM10, PM2.5, PM1, and PM0.1 resuspension due to human walking, Air. Qual. Atmos. Health (2022), https://doi.org/10.1007/s11869-022-01201-3.